The Plant Cell, Vol. 28: 2060–2078, September 2016, www.plantcell.org

Altered Transcription and Neofunctionalization of Duplicated Genes Rescue the Harmful Effects of a Chimeric Gene in *Brassica napus*

Shengqian Xia, Zhixin Wang, Haiyan Zhang, Kaining Hu, Zhiqiang Zhang, Maomao Qin, Xiaoling Dun,[1] Bin Yi, Jing Wen, Chaozhi Ma, Jinxiong Shen, Tingdong Fu, and Jinxing Tu[2]

National Key Laboratory of Crop Genetic Improvement, College of Plant Science and Technology, National Sub-Center of Rapeseed Improvement in Wuhan, Huazhong Agricultural University, Wuhan 430070, China

ORCID ID: 0000-0001-5131-4526 (J.T.)

Chimeric genes contribute to the evolution of diverse functions in plants and animals. However, new chimeric genes also increase the risk of developmental defects. Here, we show that the chimeric gene *Brassica napus male sterile 4* (*Bnams4^b*) is responsible for genic male sterility in the widely used canola line 7365A (*Bnams3 ms3ms4^{b}ms4^b*). *Bnams4^b* originated via exon shuffling ~4.6 million years ago. It causes defects in the normal functions of plastids and induces aborted anther formation and/or albino leaves and buds. Evidence of the age of the mutation, its tissue expression pattern, and its sublocalization indicated that it coevolved with *BnaC9.Tic40* (*BnaMs3*). In *Arabidopsis thaliana*, *Bnams4^b* results in complete male sterility that can be rescued by *BnaC9.Tic40*, suggesting that *BnaC9.Tic40* might restore fertility through effects on protein level. Another suppressor gene, *Bnams4^a*, rescues sterility by reducing the level of transcription of *Bnams4^b*. Our results suggest that *Brassica* plants have coevolved altered transcription patterns and neofunctionalization of duplicated genes that can block developmental defects resulting from detrimental chimeric genes.

INTRODUCTION

New genes can represent a major source of genetic innovation in genomes (Chen et al., 2010; reviewed in Chen et al., 2013; Cardoso-Moreira and Long, 2012) and may be involved in the establishment of novel biochemical pathways (Matsuno et al., 2009; Weng et al., 2012) as well as being integrated into existing gene networks (Capra et al., 2010; Chen et al., 2010, 2012b). They have been suggested to play essential roles in development (Chen et al., 2010; Ding et al., 2010), brain evolution (Chen et al., 2012a), and sexual dimorphism (Betrán et al., 2002; Ding et al., 2010). Natural chimeric genes arise from the fusion of existing sequence elements to create a new open reading frame (ORF) that contributes to novel molecular and cellular functions (Chen et al., 2013; Ding et al., 2012; Long and Langley, 1993). Most of the known chimeric genes were identified in insects and humans and were found to originate through RNA-based retrotransposition. For example, *jingwei* was generated by fusion of the N terminus of the *yellow emperor* gene with a retrotransposed *Adh* gene (Long and Langley, 1993). Although some chimeric genes induce early adaptive evolution and are finally fixed (Jones and Begun, 2005; Sayah et al., 2004; Wang et al., 2002), the majority are rapidly eliminated from the genome though pseudogenization. Only ~1.4% of chimeric genes are preserved by natural selection (Rogers et al., 2009). Most of the information on the origin, evolution, and function of chimeric genes has come from RNA-based chimeric genes than from those derived by DNA-based exon shuffling. In *Drosophila melanogaster*, 8 of 14 DNA-based chimeric genes were found to be undergoing pseudogenization or were noncoding RNA genes (Zhan et al., 2011). Although chimeric genes arise frequently in plants, their use in agricultural breeding programs has seldom been reported (Wang et al., 2006). In addition, it is not clear how plants defend themselves against the potential detrimental effects of chimeric genes.

Canola (*Brassica napus*; allotetraploid, AACC, 2n = 38) is one of the most important sources of edible oil in the Brassicaceae and was first cultivated in Europe during the Middle Ages. It was formed by natural allopolyploidization between the *Brassica oleracea* ancestor (Mediterranean cabbage, CC, n = 9) and *Brassica rapa* ancestor (Asian cabbage or turnip, AA, n = 10) (Chalhoub et al., 2014; Nagaharu, 1935). According to the "triangle of U" hypothesis, this likely occurred by natural pairwise hybridization in which three diploid *Brassica* species, *B. rapa* (AA, n = 10), *B. oleracea* (CC, n = 9), and *B. nigra* (BB, n = 8), formed the allopolyploids *B. napus* (AACC, n = 19), *B. juncea* (AABB, n = 18), and *B. carinata* (BBCC, n = 17) (Nagaharu, 1935). Such hybridization and polyploidization constitute the major driving forces of genome evolution in *B. napus* (Marhold and Lihova, 2006; Nagaharu, 1935). The *Brassica* and *Arabidopsis* lineages diverged ~20 million years ago (Mya) from a common ancestor (ancestral karyotype, n = 8) after the three polyploidization events (γ, β, and α) of angiosperms (Yang et al., 1999). Comparative genomic analyses of the 24 conserved chromosomal blocks (labeled A to X) suggested that the three basic diploid *Brassica* species descended from a common ancestor that was formed after whole-genome triplication (~15.9 Mya) (Liu et al., 2014; Lysak et al., 2005; Schranz et al., 2006; Wang et al., 2011b).

[1] Current address: Oil Crop Institute, China Academy of Agricultural Science, Wuhan 430062, China.
[2] Address correspondence to tujx@mail.hzau.edu.cn.
The author responsible for distribution of materials integral to the findings presented in this article in accordance with the policy described in the Instructions for Authors (www.plantcell.org) is: Jinxing Tu (tujx@mail.hzau.edu.cn).
www.plantcell.org/cgi/doi/10.1105/tpc.16.00281

Male sterility is the most effective and commercially significant means of using heterosis. Cytoplasmic male sterility is widely used in canola hybrid breeding. However, the genic male sterile (GMS) breeding system 7365ABC offers further advantages such as stable sterility, a wide breadth of restorer lines, and no evident negative cytoplasmic effects. Thus, this system has considerable potential to be an important approach for future hybrid breeding (Huang et al., 2012; Xia et al., 2012). The 7365ABC GMS system was discovered in the 1990s and was regarded as a natural variation (Chen et al., 1993). Many commercial hybrids based on this GMS system have since been released (Chen et al., 2002, 2003; Fan et al., 2010; Sun et al., 2004; Wang et al., 2009); for example, the winter rapeseed varieties bred using this GMS system monopolized the European rapeseed market during the 2000s. 7365ABC is controlled by two independent loci, *BnaMs3*/*Bnams3* (*BnaC9.Tic40*/ *BnaC9.tic40*) and *Bnams4*^{a}/*Bnams4*^{b}/*Bnams4*^{c} (Figure 1A). *Bnams4*^{a}/*Bnams4*^{b}/*Bnams4*^{c} is a multiallelic locus on chromosome N07, whereas *BnaMs3*/*Bnams3* is located on N19. *BnaMs3* and *Bnams4*^{a} represent suppressor genes and *Bnams4*^{b} is a male-sterile gene (Figure 1A). The dominance relationships of these alleles are *BnaMs3*>*Bnams3* and *Bnams4*^{a}>*Bnams4*^{b}>*Bnams4*^{c} (Figure 1A). The GMS system provides an excellent three-line breeding strategy for the production of commercial hybrids (Figure 1B). Thus, cloning and characterization of this multiallelic locus will be essential to understanding the biological and evolutionary mechanisms of this elite breeding system and to making better use of its potential capabilities.

The evolutionary history of this GMS system has long been recognized as an important issue for the molecular biology of reproductive development and use of heterosis in *B. napus*. Consequently, we cloned *BnaC9.Tic40* via map-based cloning (Dun et al., 2011) and showed that it encodes a protein that is a member of the translocon at the inner envelope membrane of chloroplasts (TIC) complex. BnaC9.Tic40 coordinates the participation of Tic110 and Hsp93 proteins in the translocation of specific preproteins across the inner envelope membrane into tapetal plastids (Chou et al., 2006; Chou et al., 2003; Dun et al., 2011). All *Tic40* copies from *Brassica* species can rescue the albino leaf phenotype of the *attic40* mutant of *Arabidopsis thaliana*. Only *BolC9.Tic40* from the genome C09 in *B. oleracea* and *BnaC9.Tic40* from N19 in *B. napus* can specifically rescue sterility in 7365A (Dun et al., 2014). *BnaC9.Tic40* is a gain-of-function mutation and may represent neofunctionalization among the duplicated *Tic40* homologs in *B. oleracea* lineages and has been associated with the male sterility gene *Bnams4*^{b} (Dun et al., 2014). However, the origin, evolution, and function of the sterility gene *Bnams4*^{b} remain unclear. Furthermore, the evolutionary relationship between the neofunctionalized suppressor gene *BnaC9.Tic40* and *Bnams4*^{b} is also unknown.

Our aims here were to clone *Bnams4*^{b} by map-based cloning and to characterize gene structure, expression pattern, protein function, and cell biological effects. We also examined the origin and evolutionary relationship of *Bnams4*^{b} with both suppressor genes *BnaC9.Tic40* and *Bnams4*^{a}. We found that the plants had evolved transcriptional and neofunctional mechanisms to block the developmental defects from this chimeric gene in *B. napus*.

RESULTS

Localization of *Bnams4*^{b} in a 61-kb Insertion Region

Fine mapping of *Bnams4*^{b} was performed using a population of 5500 plants from the near-isogenic line (NIL) 7365AC (*Bnams3ms3ms4*^{b}*ms4*^{c}/*Bnams3ms3ms4*^{c}*ms4*^{c}). We used the published genome data of *B. rapa* to develop simple sequence repeat and sequence characterized amplified region markers. Marker polymorphisms were identified and genetic distances were determined to narrow down the candidate physical region. Finally, the markers CL14 and DD42 (Figure 2; Supplemental Table 1) were used to delimit *Bnams4*^{b} within ~170-kb (Figure 2A), 85-kb (Figure 2B), and 78-kb (Figure 2C) DNA fragments according to the published genome sequences of *A. thaliana* (*Col-0*) (Lamesch et al., 2012), *B. rapa* (*Chiifu-401*) (Wang et al., 2011b), and *B. napus* (*Darmor-bzh*) (Chalhoub et al., 2014), respectively. The 85-kb region of *B. rapa* contained four genes, *Bra014988*, *Bra014989*, *Bra014990*, and *Bra014991* (Figure 2B); their corresponding *A. thaliana* orthologous genes were *AT3G23840*, *AT3G23900*, *AT3G23870*, and *AT3G23880* (Figure 2A). Transgenic complementation experiments with *A. thaliana* and *B. napus* plants confirmed that the corresponding four genes in 7365A were not *Bnams4*^{b}.

A mixed 7365AC genome BAC library was constructed to identify the location of *Bnams4*^{b} via chromosome landing. After screening the BAC library using the cosegregated molecular markers SD1R-SD2F (Figure 2C; Supplemental Table 1), the BAC clone B107 was identified as containing *Bnams4*^{b} (Figure 2C). We sequenced this clone using high-throughput sequencing. An additional insert fragment (~61 kb) was also identified between the molecular markers DD28 and SSR103 (Figures 2D and 2E); however, this 61-kb fragment was not present in the *Darmor-bzh* and *Chiifu-401* genome sequences (Figures 2B, 2C, and 2F). In this 61-kb region, the CC4 fragment (~8.4-kb) contained a complete heat shock protein coding sequence. A protein homologous with this sequence has been shown to interact with the Hip (HSP70-interacting protein) domain of Tic40 (a homolog of BnaTic40) (Bédard et al., 2007). Therefore, *CC4* was predicted to represent a *Bnams4*^{b} candidate gene (Figure 2E). Other genes in this candidate region were excluded as they showed no annotation related to male reproduction, no obvious phenotype after transformation, and no information regarding associated interaction with BnaC9.Tic40 (Supplemental Table 2). Subsequently, *CC4* was found to produce completely sterile anthers in all transgenic plants as well as variable frequencies of albino leaves in some plants when transformed into wild-type Col-0 *A. thaliana* (Figures 3A to 3D; Supplemental Figures 1A, 1B, and 1F). In addition, when *CC4* was transformed into 7365C plants, six plants exhibited sterile anthers (Figure 3I), but all had some albino leaves and buds (Figure 3K; Supplemental Figures 1C, 1E, and 1G). Dead buds, which occasionally appeared in 7365A sterile plants, were also observed in these transgenic plants (Figure 3K). Thus, these transgenic complementation experiments indicated that the *CC4* fragment contained the *Bnams4*^{b} gene. In addition, transgenic *A. thaliana* and *B. napus* showed higher *Bnams4*^{b} expression levels in small buds, siliques, and anthers than nontransgenic plants (Supplemental Figure 2). These male-sterile

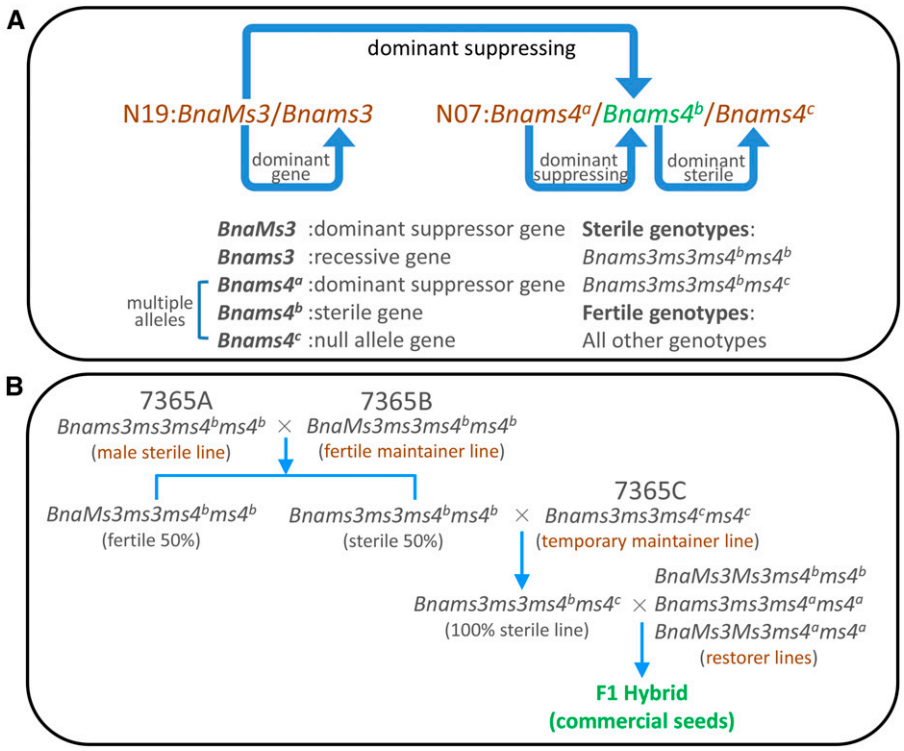

Figure 1. The Genetic Model and Three-Line Hybrid Breeding Procedure of Genic Male Sterile System 7365ABC in *B. napus*.

(A) The fertility of 7365ABC is controlled by two alleles of loci located in two different linkage groups: N07 and N19. The multigene locus (N07) consists of *Bnams4*^{a}, *Bnams4*^{b}, and *Bnams4*^{c}. *Bnams4*^{b} is a dominant male-sterile gene relative to the null allele *Bnams4*^{c}; *Bnams4*^{b} has two dominant suppressor genes *BnaC9.Tic40* and *Bnams4*^{a}. The locus N19 consists of *BnaC9.Tic40* (*BnaMs3*) and *BnaC9.tic40* (*Bnams3*). Curved blue arrows show the explicit-implicit relationships between these genes: *BnaC9.Tic40*>*BnaC9.tic40* and *Bnams4*^{a}>*Bnams4*^{b}>*Bnams4*^{c}. Therefore, only *Bnams3ms3ms4*^{b}*ms4*^{b} and *Bnams3ms3ms4*^{b}*ms4*^{c} are sterile for they have no suppressor gene, while *Bnams3ms3ms4*^{a}*ms4*^{b} and *BnaMs3ms3ms4*^{b}*ms4*^{b} are fertile as they each contain a suppressor gene. *Bnams3ms3ms4*^{c}*ms4*^{c} is also fertile as it has no sterile gene *Bnams4*^{b}, and this genotype can be used as temporary maintainer line.
(B) The genic male sterile breeding system 7365ABC consisted of male-sterile line 7365A (*Bnams3ms3ms4*^{b}*ms4*^{b}), maintainer lines 7365B (*BnaMs3ms3ms4*^{b}*ms4*^{b}) and 7365C (*Bnams3ms3ms4*^{c}*ms4*^{c}), and restorer lines (*BnaMs3Ms3ms4*^{b}*ms4*^{b} or *Bnams3ms3ms4*^{a}*ms4*^{a}, etc.). First, male-sterile line 7365A is crossed with maintainer line 7365B to generate a 1:1 ratio of fertile and sterile plants; second, the sterile plants are crossed with temporary maintainer line 7365C to generate a 100% completely sterile population; this population makes manual removal of 50% fertile plants in field during hybrid seed production of large area unnecessary, compared with using other types of genic male sterile systems. Subsequently, the 100% sterile population was extensively tested with a variety of restorer lines to produce superior hybrid seed. This kind of genic male sterile system has extensive restorer lines, compared with cytoplasmic male sterile lines, due to the wide distribution of suppressor genes (*BnaC9.Tic40* and *Bnams4*^{a}) in natural varieties or inbred lines.

phenotypes support the conclusion that the complete sequence of *CC4* contained the *Bnams4*^{b} gene.

RT-PCR and 5′- and 3′-rapid amplification of cDNA ends were used to confirm the whole gene structure of *Bnams4*^{b}. The *Bnams4*^{b} cDNA contains an 85-bp 5′ untranslated region, a 4161-bp ORF with nine exons, and a 113-bp 3′ untranslated region (Supplemental Figure 3; see Methods for gene structure confirmation). We transformed this ORF, driven by two different promoters, into *A. thaliana* and found that sterile anthers and siliques were present in transformed plants (Supplemental Figure 4), confirming that the ORF present in CC4 was *Bnams4*^{b}.

Bnams4^b Encodes a Deleterious Chimeric Protein That Localizes to Plastids

Sequence analysis of the *Bnams4*^{b} ORF revealed a fusion of three segments (AA1, AA2, and AA3) from three independent *B. napus* genes (Figure 4A). AA1, AA2, and AA3 exhibited 93.6, 93.0, and 94.1% nucleotide identities with the corresponding portions of *BnaA01g00420D*, *BnaA01g10280D*, and *BnaA01g00190D*, respectively. In contrast, another segment between AA2 and AA3 did not demonstrate homology with any reference genome sequence (Figure 4A). *BnaA01g00420D* encodes a ribonuclease III family protein located in chloroplasts; *BnaA01g10280D* encodes *pre-mRNA processing 8* (*PRP8*), which forms the conserved central component of the spliceosome (Grainger and Beggs, 2005); and *BnaA01g00190D* encodes mitochondrial *heat shock protein 70-1* (*mtHsc70-1*). None of these three genes is associated with male sterility according to the current literature. These results indicated that *Bnams4*^{b} was a newly formed functional chimeric gene composed of three segments from different genes.

In addition to male sterility, an abnormal albino or yellow leaf morphology was observed in the plants with high expression levels of *Bnams4*^{b} (Figure 4B; Supplemental Figures 1C and 1E

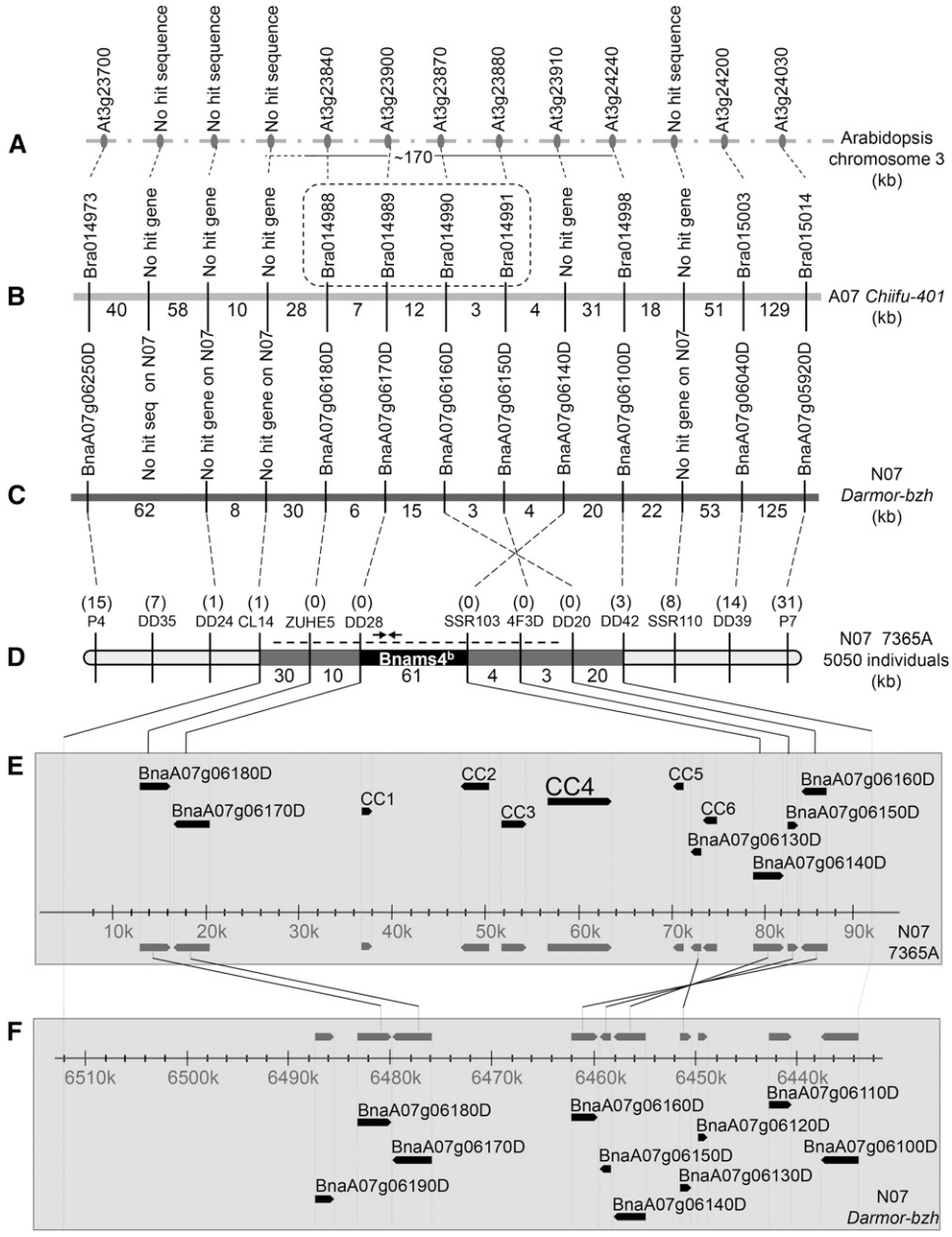

Figure 2. Physical Mapping of the Predicted Candidate Gene of *Bnams4*^{b} in *B. napus*.

(A) Corresponding *A. thaliana* chromosome 3 region homologous to the region in which *Bnams4*^{b} resides. "No hit genes" means there is no homologous *A. thaliana* gene here. The small solid ellipses indicate corresponding genes of *A. thaliana* chromosome 3 or no hit genes.

(B) Corresponding *B. rapa* chromosome A07 region homologous to the region in which *Bnams4*^{b} resides. The vertical bars indicate corresponding genes of *B. rapa* chromosome A07 or no hit genes. Dotted box represents the four predicted candidate genes for *Bnams4*^{b}.

(C) Corresponding *B. napus* chromosome N07 region homologous to the region in which *Bnams4*^{b} resides. The vertical bars indicate corresponding genes of *B. napus* chromosome N07 or no hit genes.

(D) Genetic and physical maps of *Bnams4*^{b}. The numbers in parentheses above the molecular marker names indicate the number of recombinants of corresponding markers. Primer pair SD1R-SD2F and the BAC clone B107 are represented by the black arrows and the dotted line, respectively.

(E) Schematic view of genes in the candidate interval on 7365A chromosome N07. Six homologous Darmor-*bzh* genes are indicated. *CC4* is the candidate gene for *Bnams4*^{b}.

(F) Schematic view of genes in the corresponding interval on Darmor-*bzh* chromosome N07. Ten Darmor-*bzh* genes are indicated.

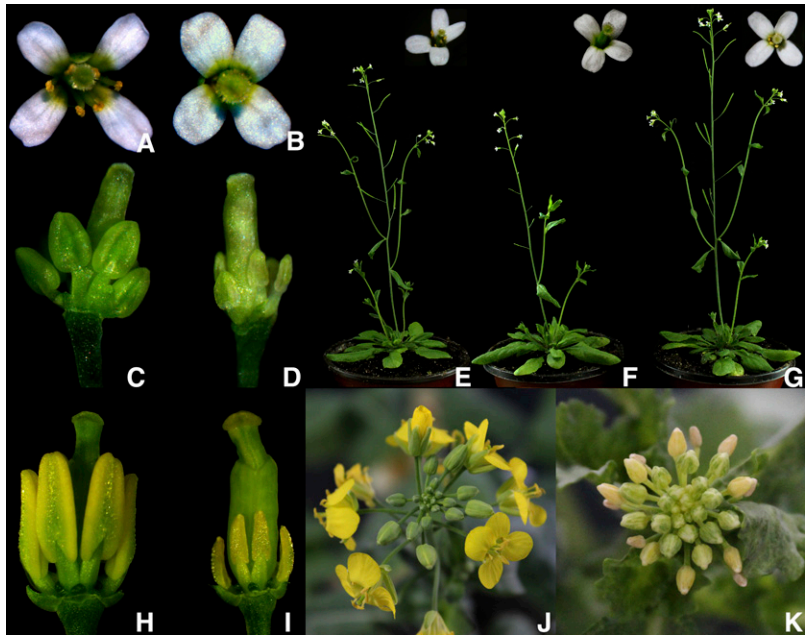

Figure 3. Phenotype of Transformed Wild-Type *A. thaliana* and Transformed 7365C with Candidate Sequence CC4.

(A) and **(B)** Open flowers of wild-type and CC4 transgenic *A. thaliana*.
(C) and **(D)** Buds with removed perianth of wild-type (left) and CC4 transgenic *A. thaliana* (right).
(E) *BnaC9.Tic40* can restore the male sterility caused by *Bnams4*^{b} in *A. thaliana*. Complete fertile anther appeared in the F1 plant both contained *BnaC9.Tic40* and *Bnams4*^{b}.
(F) Sterile anther appeared in the F2 segregated plants which only contained *Bnams4*^{b}.
(G) Wild-type *A. thaliana* grown under the same conditions.
(H) and **(I)** Buds with removed periapts of 7365C (left) and CC4 transgenic *B. napus* (right).
(J) and **(K)** Inflorescence of 7365C and CC4 transgenic *B. napus*.

to 1G). RT-qPCR and promoter GUS analyses revealed that *Bnams4*^{b} was predominantly expressed in rosette leaves, cauline leaves, anthers, and siliques (Figures 4C and 4D). The variable frequencies of albino leaves resulted from different levels of *Bnams4*^{b} transcription and translation in *Bnams4*^{b}-transgenic *B. napus* plants (Figure 4B). In contrast, the mutant 7365A plants exhibited normal green leaves despite *Bnams4*^{b} expression (Figure 4C), indicating that the leaves were subjected to a dose-dependent effect of *Bnams4*^{b} expression (Figure 4B). The albino or yellow leaf phenotype was consistent with the chloroplast localization observed in an *A. thaliana* protoplast transformation assay (Figure 4E) and with *Agrobacterium tumefaciens*-mediated transient expression in tobacco leaf epidermal cells (Supplemental Figure 5). These data suggested that the Bnams4^{b} protein has a deleterious effect in both anthers and leaves.

Bnams4^{b} Affects the Normal Function of Plastid to Cause Aborted Anther and Albino Leaves

To investigate how *Bnams4*^{b} caused aborted development of anthers, we used semi-thin sections and transmission electron microscopy (TEM) to investigate anther development in 7365A plants. Initiation of the abnormal phenotype occurred at the premeiosis stage and progressed to the tetrad stages (Supplemental Figures 6G and 6H). TEM revealed subtle differences in the vacuolar tapetum and microspores: defective biosynthesis of exine (Supplemental Figures 7F2 and 7H2); surrounded microspores throughout the development of the primary cell wall (Supplemental Figures 7H2 and 7J2); vacuolated tapetal cells and microspores (Supplemental Figures 7D1, 7D2, and 7F2); and reduced number of plastids, tapetosomes, and elaioplasts in tapetal cells (Supplemental Figures 7D3, 7F4 and 7J3). Ultimately, disintegration of the tapetal cells occurred in sterile anthers (Supplemental Figures 7H3, 7J1, and 7J3). The abnormal function of the tapetal plastids caused by *Bnams4*^{b} in the premeiotic and tetrad stages thus led to anther abortion.

Overexpression of *Bnams4*^{b} in wild-type Col-0 *A. thaliana* caused variable degrees of leaf albinism. Albino leaves exhibited few starch grains in their chloroplasts and insufficiently developed thylakoids (Figure 5A), indicating that *Bnams4*^{b} overexpression caused aberrant chloroplast development. To further ascertain the effects of *Bnams4*^{b} on chlorophyll synthesis, a leaf chlorophyll meter and photometric measurement of solvent-extracted chlorophyll were used to measure chlorophyll concentrations in albino *A. thaliana* leaves. Both methods indicated significantly lower absolute chlorophyll content in albino leaves than in wild-type green leaves (Figure 5B). Together, these results suggested that Bnams4^{b} might block fatty acid synthesis in tapetal plastids as well as chlorophyll synthesis in leaf chloroplasts.

Scanning electron microscopy revealed that the sterile anthers of NIL 7365AC exhibited a relatively smooth epidermis (Figure 5A).

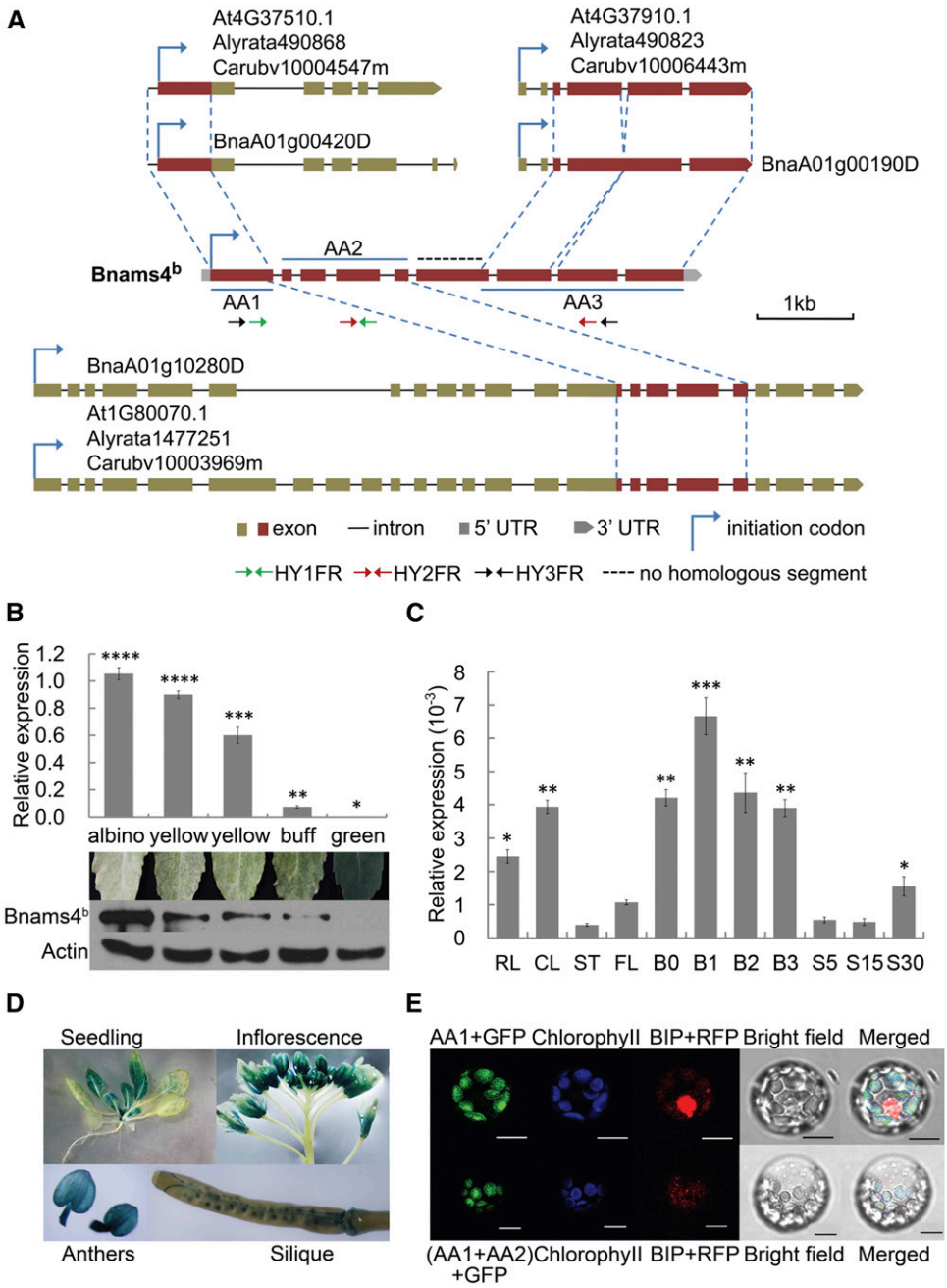

Figure 4. Gene Structure, Expression Pattern, and Subcellular Localization of *Bnams4*^{b}.

(A) The structure of *Bnams4*^{b} consists of four parts: portions of three genes and a segment (black dashed line) with no homologous sequences in four reference genome sequences.

(B) Gradient expression of *Bnams4*^{b} in leaves with varying degrees of albino phenotypes in *Bnams4*^{b} transgenic *B. napus*. Albino leaves had the highest expression level while green leaves almost had no expression of *Bnams4*^{b}. Immunoblotting of *Bnams4*^{b} showed the same tendency as transcript levels. Error bars indicate SD. The Duncan's multiple-range test ($P < 0.05$, SPSS version 19.0) was used to investigate the significant differences of average relative expressions of the five samples. Different numbers of asterisks between two random samples indicated they have significant difference with means of relative expressions; same numbers mean no significant difference between them.

(C) RT-qPCR analysis of *Bnams4*^{b} in sterile plants of NIL 7365AC. RL, rosette leaves; CL, cauline leaves; ST, stems; FL, flowers; Bud0, bud of 0 to 1 mm; Bud1, bud of 1 to 2 mm; Bud3, bud of 3 to 4 mm; Bud4, bud of 4 to 5 mm; SD5, siliques 5 d after pollination; SD15, siliques 15 d after pollination; SD30, siliques 30 d after pollination. Error bars indicate SD. The Duncan's multiple-range test ($P < 0.05$, SPSS version 19.0) was also used to investigate the significant differences between various tissues.

(D) GUS analysis of *Bnams4*^{b} in transgenic wild-type *A. thaliana*.

Gas chromatography-mass spectrometry and gas chromatography-flame ionization detection (Bonaventure et al., 2004; Franke et al., 2005) revealed that the total wax and cutin contents decreased considerably in the sterile anthers compared with fertile anthers, regardless of the anther developmental stage (Figure 5C). Consistent with this, mid-chain fatty acids such as C16:0, C16:3, C18:2, and C18:3 (Figure 5D), which represent the main constituents of the total wax, were also reduced. Cutin monomer analysis of the sterile anther epidermis demonstrated significant reductions in C14:0, C16:0, C18:0, C16:3, C18:2, and C18:3 fatty acids in addition to a low abundance of components such as C16:0 DFA, C19:0 DFA, C18:1 DFA, C16:0 (9,10)-HDFA, C18:1-ω-HFA, and C18:1 (9,10)-EPOXY-ω-HFA (Figure 5E). Plastids are the most important subcellular organelles for C16 and C18 fatty acid synthesis. These results suggested that *Bnams4^b* might affect lipid synthesis systems in the tapetal plastid.

Bnams4^b Originated from Duplicated Genes by Exon Shuffling

We next attempted to compare *Bnams4^b* with its orthologous genes in *Capsella rubella*, *Arabidopsis lyrata*, and *A. thaliana* to investigate the possible mechanism by which *Bnams4^b* originated. *C. rubella* (n = 8) and *A. lyrata* (n = 8) were included in this analysis to increase the representation of Brassicaceae ancestral karyotypes (n = 8) (Figure 6A) (Koch and Kiefer, 2005; Lysak et al., 2006; Yogeeswaran et al., 2005). The results indicated that *Bnams4^b* arose via the fusion of segments of three independent *C. rubella*, *A. lyrata*, and/or *A. thaliana* genes: *Carubv10004547m*/*Alyrata490868*/*At4g37510.1*, *Carubv10003969m*/*Alyrata1477251*/*At1g80070.1*, and *Carubv10006443m*/*Alyrata490823*/*At4g37910.1* (Figure 4A). At least two exon-shuffling events occurred during the process of *Bnams4^b* formation. Additionally, the sixth exon of *Bnams4^b* consisted of an unidentified sequence that might have been recruited by the AA3 segment (Figure 4A). These data suggested that *Bnams4^b* had a complex origin and likely arose from multiple exon shuffling events.

Phylogenetic analysis of AA1, AA2, and AA3 showed that *Bnams4^b* had high sequence similarity with *Brams4^b-40* (Supplemental Figure 8) and *Bol029014* (from Bolbase, http://www.ocri-genomics.org/bolbase/) (Supplemental Figure 9). Amino acid sequence alignment suggested that Bol029014, Brams4^b-40, and Bnams4^b represent highly similar orthologs that exhibited different transcript structures (Supplemental Figure 9 and Supplemental Table 3). In addition, an ~490-amino acid deletion was identified in Bol029014 (Supplemental Figure 9). AA1, AA2, and AA3 all exhibited higher sequence similarity to Brams4^b-40 than to Bol029014 in *B. oleracea* (Supplemental Figure 8), suggesting that *Bnams4^b* was directly derived from its orthologous gene in *B. rapa* rather than from its orthologous gene in *B. oleracea*. Additionally, AA1, AA2, and AA3 were shown to have corresponding paralogous gene fragments in *B. rapa* and *B. oleracea* (AA1, *Bra011770* and *Bol028906*; AA2, *Bra021701*, *Bra013431*, *Bol004508*, and *Bol000723*; AA3, *Bra010620*, *Bra011794*, *Bol032741*, and *Bol028880*). This indicated that *Bnams4^b* was generated from the DNA fragments of duplicated genes in *Brassica*.

To further confirm that *Bnams4^b* was derived from *B. rapa*, the full-length cDNAs and genomic sequences of the identified *ms4^b* genes of *Brassica* species were isolated. A phylogenetic tree was constructed using the full-length ORFs of 13 *Bnams4^b* homologs (Supplemental Data Set 1). The 13 ORFs were distributed into two lineage groups: a *B. oleracea* group and a group that included *B. rapa*, *B. napus*, and *B. juncea* (Figure 6D). *Bnams4^b* exhibited the highest sequence similarity to *Bnams4^b-112*, *Bjums4^b-88*, and *Brams4^b-40*. The other four homologs in *B. oleracea*, all of which lacked the 490 amino acid region, were clustered into the *B. oleracea* group (Figure 6D). This analysis suggested that the *Bnams4^b* homologs in *B. napus* and *B. juncea* might have been derived from *B. rapa*.

Bnams4^b Is a Relatively Young Gene and Not Completely Fixed in *B. napus*

According to the U-triangle theory, *B. rapa* (AA; n = 10) and *B. oleracea* (CC; n = 9) were the parental species for the derivative allotetraploid species, *B. napus* (AACC; n = 19) (Nagaharu, 1935). Therefore, we investigated whether these species contained the intact sequence or partially combined fragments of *Bnams4^b*. Three pairs of degenerate primers were used to amplify two of the three segments of *Bnams4^b*: AA1, AA2, and AA3 (Figure 4A; Supplemental Table 1). For example, the degenerate primer pair HY1F and HY1R was used to specifically amplify the chimeric structure between AA1 and AA2 (based on the presence/absence of specific PCR fragment bands). The degenerate primer pairs were used to screen 30 lines of *B. oleracea*, 23 lines of *B. rapa*, 7 lines of *B. nigra*, 200 lines of *B. napus*, 10 lines of *B. juncea*, and 20 lines of *B. carinata* (Supplemental Data Set 1). However, we found no partially combined fragments (e.g., AA1+AA2, AA2+AA3, or AA1+AA3) in these lines. The intact sequence of *Bnams4^b* was only present in *B. oleracea* (16/30), *B. rapa* (14/23), *B. napus* (123/200), and *B. juncea* (8/10), whereas it did not appear in *B. nigra* (0/7) or *B. carinata* (0/20) (Figure 6A). These findings indicated that *Bnams4^b* might have originated after the divergence of *B. nigra* and *B. oleracea*, which has been suggested to occur <8 Mya (Figure 6A) (Liu et al., 2014; Lysak et al., 2005). Therefore, *Bnams4^b* represents a relatively young chimeric gene.

Bnams4^b was not found in all *B. napus* lines, suggesting that it had not been completely fixed in this species. Therefore, the gene frequencies of two loci (*BnaMs3*/*Bnams3* and *Bnams4^a*/*Bnams4^b*/

Figure 4. (continued).

(E) Subcellular localization of Bnams4^b protein in *A. thaliana* leaf protoplasts. For the five images above, from left to right, the GFP signal of AA1-GFP fusion construct, blue fluorescence which was transformed from the chlorophyll red autofluorescent signal, red fluorescent signal of endoplasmic reticulum marker, the images in bright field, and merged images of the above all. Five images below indicated the sublocalization of (AA1+AA2)-GFP fusion construct with the same order of notes as *Bnams4^b* AA1-GFP fusion construct. Bars =10 μm.

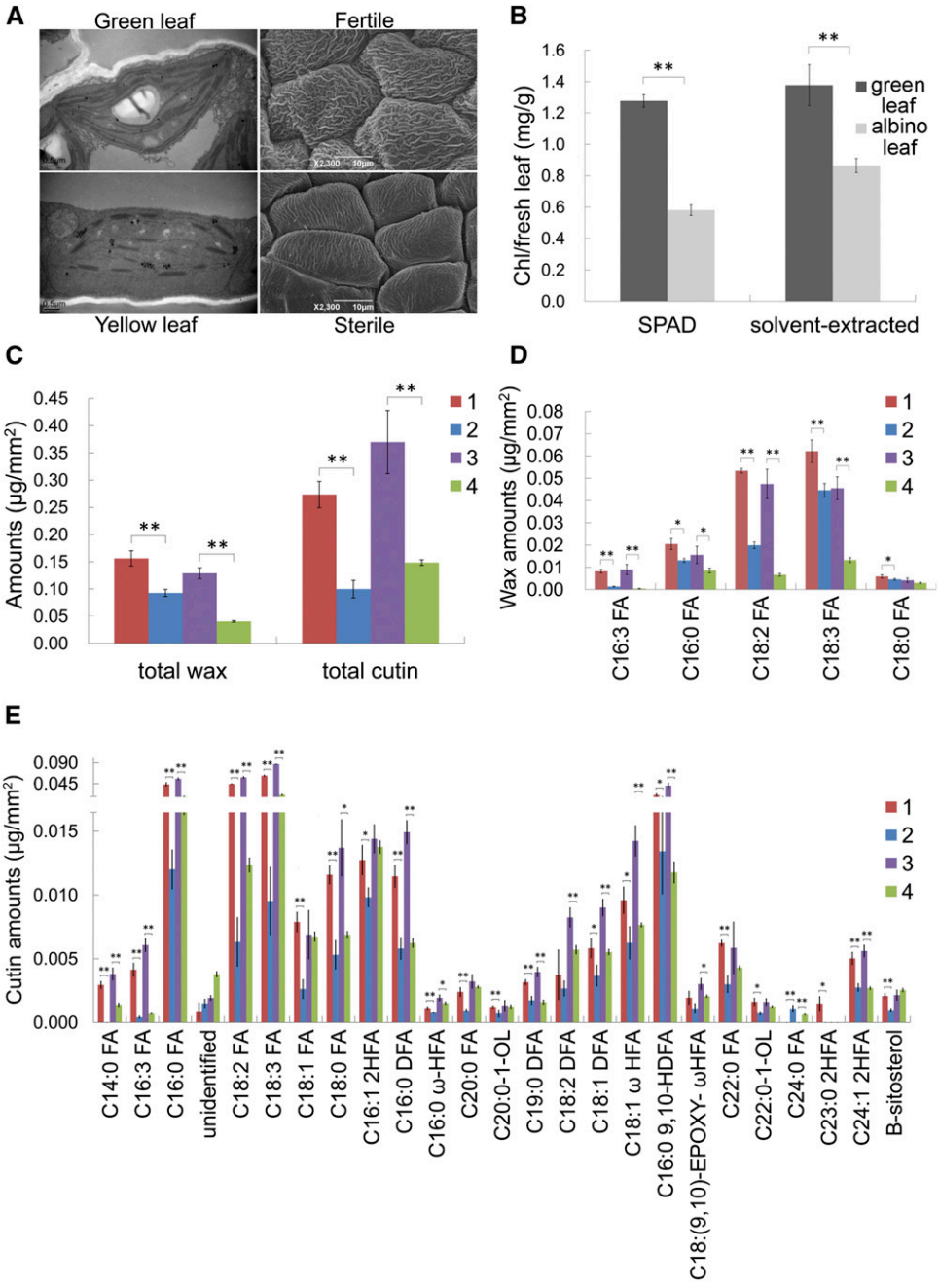

Figure 5. Chlorophyll, Cutin, and Wax Measurements of Sterile and Fertile Anthers and Leaves.

(A) TEM observations of chloroplast in *Bnams4*^{b} transgenic *B. napus* leaf and normal green leaf of 7365C (left). Scanning electron microscopy observations of fertile and sterile anther epidermis in NIL 7365AC (right).

(B) Chlorophyll content determination of albino leaves (*Bnams4*^{b} transgenic) and green leaf (wild type) in *A. thaliana*. "SPAD" and "Solvent-extracted" represent two different methods of measurement.

(C) Comparison of total wax and cutin contents per unit surface area between fertile and sterile anther.

(D) Analysis of C16/C18 fatty acid wax components in the fertile and sterile anther epidermis.

(E) Analysis of cutin constituents in the fertile and sterile anther epidermis. Asterisks indicate components with significant difference between sterile and fertile anthers. 1, Anthers of *Bnams3ms3ms4*^{c}*ms4*^{c} fertile plant with 2- to 3-mm buds; 2, anthers of *Bnams3ms3ms4*^{b}*ms4*^{c} sterile plant with 2- to 3-mm buds; 3, anthers of *Bnams3ms3ms4*^{c}*ms4*^{c} fertile plant with 4- to 5-mm buds; 4, anthers of *Bnams3ms3ms4*^{b}*ms4*^{c} sterile plant with 4- to 5-mm buds. All data represent mean ± SD. *P < 0.05 and **P < 0.01. Data were subjected to one-way ANOVA F test for each parameter.

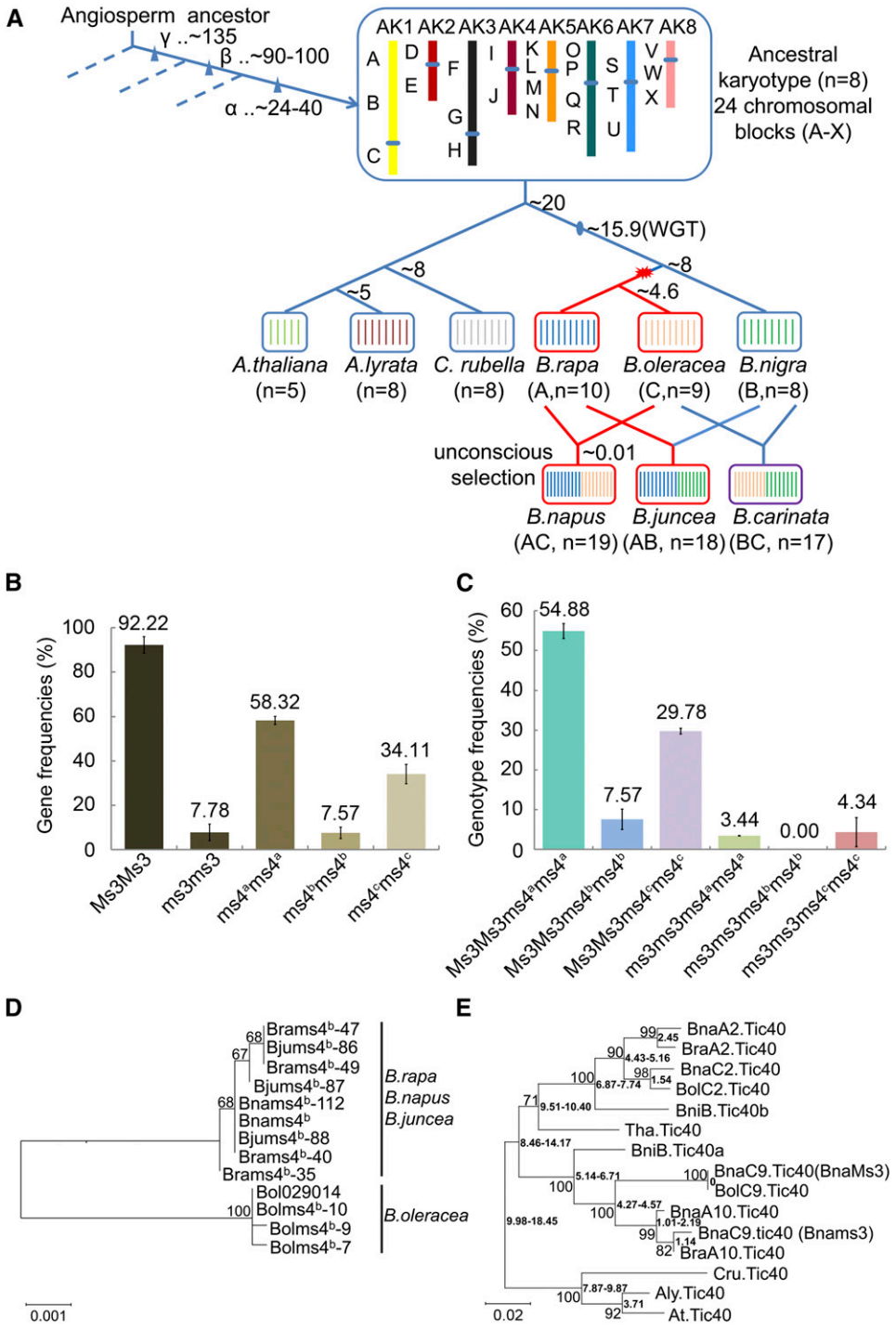

Figure 6. The Age, Genes Frequencies, and Phylogenetic Relationship Analysis of *Bnams4*^{b} and Divergence Time Estimations of Tic40 Homologies.

(A) Phylogeny and species differentiation times of certain *Brassica* and *Arabidopsis* lineages. Light-blue triangles represent the evolution of angiosperms three polyploidization events. Light-blue oval indicated the whole genome triplication (WGT) of *Brassica*. The vertical lines in the boxes represent the chromosome numbers of the haplotype. Red breaking symbol indicated the estimated time of *Bnams4*^{b} generation. Red boxes and lines indicated evolutionary path of the *Bnams4*^{b} gene. The six boxes in the lower right corner showed U's triangle theory, which indicated *B. napus* was formed by natural hybridization of *B. rapa* and *B. oleracea*. Time unit is millions of years ago.

(B) Gene frequencies of two gene loci (*Bnams4a*/*Bnams4*^{b}/*Bnams4*^{c} and *BnaMs3*/*Bnams3*) in two populations of *B. napus*. Different numbers of asterisks indicated significant differences between different gene frequencies (Duncan's multiple-range test, $P < 0.05$, SPSS version 19.0). Data represent mean ± SD.

Bnams4^{c}) and the genotype frequencies were investigated using linked molecular markers in the 200 lines from the above analysis plus an additional 148 inbred lines. The genotype frequencies of the suppressor genes *BnaMs3Ms3* (92.22%) and *Bnams4*^{a}*ms4*^{a} (58.32%) were higher than for the sterility gene *Bnams4*^{b}*ms4*^{b} (7.57%) (Figure 6B). The genotype frequencies of *BnaMs3Ms3ms4*^{a}*ms4*^{a} and *BnaMs3Ms3ms4*^{c}*ms4*^{c} were also significantly higher than other genotypes whereas the sterile genotype had zero frequency (Figure 6C). These results indicated that the sterility gene *Bnams4*^{b} was present at a low frequency while the two suppressor genes *BnaC9.Tic40* and *Bnams4*^{a} showed higher gene frequencies due to their stronger adaptive properties in *B. napus*. Therefore, we speculate that *Bnams4*^{b} is a detrimental chimeric gene whose existence depends on the widespread suppressor genes *BnaC9.Tic40* and *Bnams4*^{a}.

Bnams4^{b} Coevolved with the Suppressor Gene *BnaC9.Tic40*

The neofunctionalization of *BnaC9.Tic40* (*BnaMs3*) is restricted to *B. oleracea* and its derivative species (such as *B. montana*, *B. villosa*, *B. carinata*, and *B. napus*) (Dun et al., 2014). Thus, neofunctionalization likely occurred after the divergence of the *Brassica* A, B, and C genomes (Dun et al., 2014). *Bnams4*^{b} was generated between the time of *B. nigra* divergence from the *Brassica* lineage and the divergence of *B. rapa* and *B. oleracea* (Figure 6A). These data suggested that the sterility gene *Bnams4*^{b} and the suppressor gene *BnaC9.Tic40* probably coevolved in *B. oleracea* and its derivatives. Tic40 is an ancient conserved molecular chaperone that transfers nuclear-encoded proteins into the chloroplast, and its orthologs exist in nearly every green plant species. We attempted to estimate the age of *BnaC9.Tic40* based on the synonymous (Ks) substitution rate. Using the DnaSP program, the age of *BnaC9.Tic40* was estimated at 4.27 to 4.57 Mya (Figure 6E; Supplemental Data Set 2). The estimated divergence times of *Brassica* species as determined by Ks corresponded with those reported in previous studies. For example, the divergence of the *Arabidopsis* and *Brassica* lineages in the current study was 9.98 to 18.45 Mya versus the reported 14.5 to 20.4 Mya (Yang et al., 1999), that of *B. nigra* and *B. oleracea* was 6.87 to 7.74 Mya versus the reported 7.9 Mya (Lysak et al., 2005), that of *B. oleracea* and *B. rapa* was 4.43 to 5.16 Mya versus the reported 4.6 Mya (Liu et al., 2014), that of *A. thaliana* and *A. lyrata* was 3.71 Mya versus the reported 5 Mya (Koch and Matschinger, 2007), and that of *A. thaliana* and *C. rubella* was 7.87 to 9.87 Mya versus the reported 8 Mya (Franzke et al., 2009; German et al., 2009) (Figure 6E). We also calibrated the molecular clock to estimate the divergence time (functional differentiation time) between *BnaC9.Tic40* and *BnaC9.tic40*. The estimated divergence time of *BnaC9.Tic40* using MEGA package software was 4.45 Mya (Supplemental Figure 10). In conclusion, the estimated age of *BnaC9.Tic40* (4.27 to 4.57 Mya or 4.45 Mya) essentially coincided with the time at which *Bnams4*^{b} originated. Therefore, we speculate that the detrimental gene *Bnams4*^{b} might have coevolved with the suppressor gene *BnaC9.Tic40*.

BnaC9.Tic40 Rescues the Sterility Caused by *Bnams4*^{b} in *A. thaliana*

The presence of the *Bnams4*^{b} gene caused complete male sterility in *A. thaliana* (Figures 3B and 3D). We performed a genetic transformation experiment to investigate whether *BnaC9.Tic40* was able to restore male fertility. First, *BnaC9.Tic40* and *Bnams4*^{b} were individually transformed into wild-type Col-0 *A. thaliana*. Subsequently, sterile plants expressing *Bnams4*^{b} were used as the female parent for hybridization with *BnaC9.Tic40*-transgenic plants. F1 plants containing both *BnaC9.Tic40* and *Bnams4*^{b} had completely fertile anthers (Figure 3E; Supplemental Table 4), indicating that *BnaC9.Tic40* completely rescued the sterility caused by *Bnams4*^{b} in *A. thaliana*. Fertility segregation was analyzed in an F2 population derived from a few F1 plants; most plants had a male fertile phenotype, and only a few were sterile due to the presence of multiple copy numbers of the transgene or the negative effect of *Bnams4*^{b} (Figure 3F; Supplemental Table 4). Therefore, the pollination control system of 7365AB was successfully reconstructed in *A. thaliana*, indicating that the BnaC9.Tic40 protein in plastids could block the detrimental defect of the chimeric Bnams4^{b} protein during anther development. It is possible that *Bnams4*^{b} and *BnaC9.Tic40* could potentially be used for utilization of heterosis in other species.

Bnams4^{a} Rescues Fertility by Reducing the Transcriptional Level of the Chimeric Gene

Comparative sequencing showed that the core promoter, nine exons, and eight introns showed no critical differences between *Bnams4*^{b} and the chimeric gene in the *Bnams4*^{a}*ms4*^{a} genotype. The chimeric gene sequence corresponding to the *Bnams4*^{a}*ms4*^{a} genotype contained two single nucleotide polymorphisms (SNPs) compared with the ORF of *Bnams4*^{b} (one in the fourth intron and another synonymous SNP in the seventh exon) (Figure 7A). However, these two SNP differences in the *Bnams4*^{a}*ms4*^{a} genotype resulted in consistent anther sterility with the *Bnams4*^{b} gene in *A. thaliana* (Supplemental Figure 11). As there was no hAT-type miniature inverted repeat transposable element (hAT-MITE) in the *Bnams4*^{a}*ms4*^{a} genotype (Figure 7A), we explored transcript levels of the *Bnams4*^{a}*ms4*^{a} chimeric ORF and the

Figure 6. (continued).

(C) Genotype frequencies in two populations of *B. napus* with same analysis as in **(A)**.

(D) The phylogenetic tree for *Bnams4*^{b} homologs in the Brassicaceae. The full-length ORF sequences of *Bnams4*^{b} homologs were used for phylogenetic analysis using MEGA4.0. Bna, *B. napus*; Bol, *B. oleracea*; Bra, *B. rapa*; Bni, *B. nigra*. The numbers on nodes are bootstrap values.

(E) Divergence time estimations of Tic40 homologies by Ks value, which indicated that the divergence time of *BnaC9.Tic40* and *BnaC9.tic40* is between 4.27 and 4.57 Mya, which is consistent with the age of *Bnams4*^{b} (~4.6 Mya). The estimated divergence time between other genes was also consistent with the previous studies (see Results).

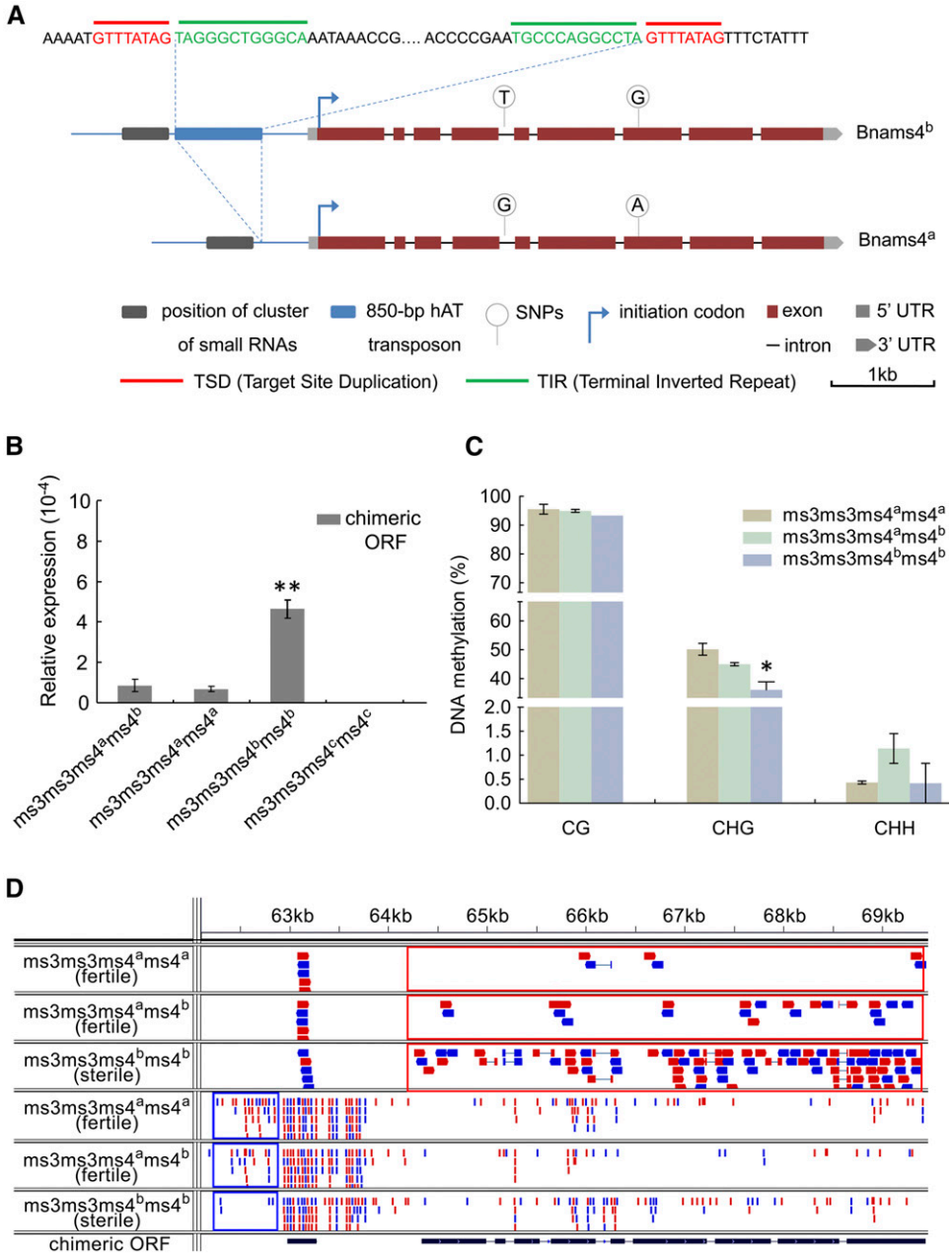

Figure 7. *Bnams4*^{a} Probably Rescued the Sterility by Suppressing Expression of the Chimeric ORF.

(A) Structure comparison of the chimeric genes in *Bnams3ms3ms4*^{a}*ms4*^{a} (*Bnams4*^{a}*ms4*^{a}-chimeric-ORF) and *Bnams3ms3ms4*^{b}*ms4*^{b} (*Bnams4*^{b}) from NIL 736512AB. It shows an insertion of 850-bp MITE in the *Bnams4*^{b} regulatory region but not in regulatory region of the *Bnams4ams4a*-chimeric-ORF. Although there are two SNPs between *Bnams4*^{a}*ms4*^{a}-chimeric-ORF and *Bnams4*^{b}, both of them can lead to male sterility in *A. thaliana*. This suggests both the chimeric ORF in *Bnams3ms3ms4*^{a}*ms4*^{a} and *Bnams3ms3ms4*^{b}*ms4*^{b} are functional in causing sterility.

(B) The transcript level of the chimeric ORF in three kinds of genotypes from self-crossing of fertile individuals in NIL 736512AB. By self-crossing, the fertile individuals in NIL 736512AB produced three genotypes: *Bnams3ms3ms4*^{a}*ms4*^{a} (fertile), *Bnams3ms3ms4*^{a}*ms4*^{b} (fertile), and *Bnams3ms3ms4*^{b}*ms4*^{b} (sterile). The anthers from about the tetrad stage (buds of 1.5 to 2 mm) were used for analysis. 7365C (*Bnams3ms3ms4*^{c}*ms4*^{c}) which did not contain *Bnams4*^{b} was used as negative control.

(C) DNA methylation analysis of the small RNA regions of *Bnams4*^{a}*ms4*^{a}-chimeric-ORF and *Bnams4*^{b} by bisulphite-based method. It shows methylation level of CHG type is higher in the small RNAs region of *Bnams4*^{a}*ms4*^{a}-chimeric-ORF than the sterile genotype: *Bnams3ms3ms4*^{b}*ms4*^{b}. All data represent mean ± SD. *$P < 0.05$.

Bnams4^b gene in three genotypes, namely, *Bnams3ms3ms4*^{a}*ms4*^{a}, *Bnams3ms3ms4*^{a}*ms4*^{b}, and *Bnams3ms3ms4*^{b}*ms4*^{b}, that were generated by self-crossing of heterozygous individuals (*Bnams3ms3ms4*^{a}*ms4*^{b}) in NIL 736512AB (Xia et al., 2012). The transcript levels were significantly higher in the sterile anthers than in the fertile anthers of two genotypes (Figures 7B and 7D), indicating that expression of *Bnams4*^{b} and *Bnams4*^{a}*ms4*^{a}-chimeric-ORF was reduced by *Bnams4*^{a}. Furthermore, small RNA sequencing revealed that *Bnams4*^{a} was able to produce a cluster of small RNAs (21 to 24 nucleotides) in the regulatory region of the *Bnams4*^{a}*ms4*^{a}-chimeric-ORF (Figure 7D). We speculated that these small RNAs might block transcription of *Bnams4*^{b} and *Bnams4*^{a}*ms4*^{a}-chimeric-ORF by RNA-directed DNA methylation (Figure 7C; Supplemental Figure 12). In addition, the candidate region for *Bnams4*^{c} in 7365C did not contain the 61-kb segment, indicating that *Bnams4*^{c} was a null allele (Supplemental Figure 13).

DISCUSSION

In this study, *Bnams4*^{b} was found to be a relatively young chimeric gene (~4.6 to 8 Mya) formed by the fusion of partially duplicated segments (AA1, AA2, and AA3) of three independent genes through exon shuffling events (Figure 4A). Overexpression of *Bnams4*^{b} caused yellow or albino leaves that were regarded as representing various degrees of lethal effect (Figure 4B). This dominant function is in contrast to the general functioning of newly evolved genes observed in animals. Many new genes in Drosophila rapidly become essential for organ formation and patterning, as demonstrated by the high probability of lethality in the pupal and larval stages following their knockdown (Chen et al., 2010). In mammals, the newly evolved genes *FGF4* (Parker et al., 2009), *SRGAP2C* (Dennis et al., 2012), *CYPA* (Sayah et al., 2004), and *POLDI* (Heinen et al., 2009) also contribute to essential functions in development and disease resistance providing them with an adaptive evolutionary advantage and enabling their subsequent fixation. In contrast, *Bnams4*^{b} is not fixed and is of relatively recent origin. Consistent with this, *Bnams4*^{b} has almost no intraspecific nucleotide variation (Supplemental Table 3) and is thus not suitable for rigorous statistical analysis since the few observable sequence changes are not sufficient to support powerful statistical testing (Supplemental Table 5). Nevertheless, a Ka/Ks ratio for *Bnams4*^{b} is smaller than 1 (0.57752), which was calculated using the CODEML program of the Phylogenetic Analysis by the Maximum Likelihood statistical package (Goldman and Yang, 1994; Zhang et al., 2011) (to test the possibility of functional constraints; Supplemental Table 6), supporting its functionality. As an artificially selected gene for breeding, it can be maintained in the population at detectable levels despite its slight detrimental effects. This differs from naturally existing new genes whose existence depends on the positive selection of advantageous functions. The identification of a functional constraint is interpreted to mean that the gene product has certain functions valuable for the wild-type species that permits its retention over a substantial period prior to its identification and utilization.

Bnams4^b encodes a novel chimeric protein that causes anther abortion and albino leaves, which are detrimental to reproduction and vegetative growth. However, plants evolved two patterns to prevent these unfavorable effects. The suppressor gene *Bnams4*^{a} altered transcription levels of *Bnams4*^{b} while *BnaC9.Tic40* showed a coevolutionary protein-level epistatic control of *Bnams4*^{b}. The neofunctionalization of *BnaC9.Tic40* within *B. oleracea* enabled the new function of restoring fertility (Dun et al., 2014). *BnaC9.Tic40* constitutively expressed primarily in seedlings, leaves, anthers, siliques, and seeds and localized in the chloroplast (Dun et al., 2011). This pattern of expression is similar to that of *Bnams4*^{b} (Figures 4C to 4E). Additionally, the identified age of *BnaC9.Tic40* is also consistent with the estimated age of *Bnams4*^{b} (Figures 6A and 6E). These consistent results indicate that coevolution probably enabled the persistence of Bnams4^b, based on a complex protein interaction network (but not a direct protein interaction; see Supplemental Figure 14) involving BnaC9.Tic40 that rescues sterility by a coevolutionary protein-level pattern. By contrast, *Bnams4*^{a} was shown to act by reducing the level of *Bnams4*^{b} expression. According to those further results (Figure 7), we speculated that the hAT-MITE close to the small RNAs site is not present in the regulatory region, resulting in the normal synthesis of small RNAs in *Bnams3ms3ms4*^{a}*ms4*^{a} plants. These small RNAs might induce RNA-directed DNA methylation to suppress the transcription of the chimeric ORF and thereby rescue sterility. Anyway, *Bnams4*^{a} rescues the sterility by a transcriptional pattern. The capacitor theory indicated that some genes can serve as buffering capacitor for genetic variation (Rutherford and Lindquist, 1998), and it has been applied to *A. thaliana* (Queitsch et al., 2002), Drosophila (Sollars et al., 2003), yeast (Jarosz and Lindquist, 2010), and cavefish (Rohner et al., 2013). *BnaC9.Tic40* and *Bnams4*^{a} can buffer the detrimental genetic variation (male sterility). Under the protection of the buffer genes, the genetic change behaves like neutral variant. Once *BnaC9.Tic40* is changed to *BnaC9.tic40* or *Bnams4*^{a} disappears, the detrimental effect (male sterility) was then exposed. Our results may suggest that *BnaC9.Tic40* and *Bnams4*^{a} act as standing capacitors in an evolutionary time scale for the genetic variation through genetic and epigenetic mechanisms, respectively.

By destroying tapetal plastids and chloroplasts, *Bnams4*^{b} caused a reduction in unsaturated C16/C18 fatty acids and induced abnormal chlorophyll synthesis (Figures 5B to 5E). However, this gene differs from the previously reported genes implicated in cutin- and sporopollenin-defective mutants (Chen et al., 2011; de Azevedo Souza et al., 2009; Li et al., 2010; Shi et al.,

Figure 7. (continued).

(D) Integrative Genomics Viewer screen capture of RNA-seq reads mapping to chimeric ORF. The three panels above showed transcriptome sequencing reads (~100 bp), while three panels below represented microRNA sequencing reads (~21 to 24 bp). These results suggested that a cluster of microRNA (blue box) in promoter region might repress the expression of chimeric ORF (red box). Both sense (represented in red) and antisense (represented in blue) strand reads are shown.

2011), which all encode lipid biosynthesis-related enzymes. Instead, *Bnams4*^{b} mainly consists of three segments (AA1, AA2, and AA3) that exhibit high similarity with three *A. thaliana* genes: *AT4G37510*, a ribonuclease III family protein; *AT1G80070*, a component of the spliceosome; and *AT4G37910*, known as *mtHsc70-1*. AA1 appeared to encode an N-terminal chloroplast transit peptide, whereas AA2 was homologous to the partial sequence of *AT1G80070*, whose null mutations were shown to lead to embryonic lethality and abnormal suspensor development (Schwartz et al., 1994). AA3 contained an intact HSP70 functional domain. None of these segments has been individually implicated in lipid biosynthesis or male sterility. Therefore, we speculate that the AA2 and AA3 protein had been mistransferred into the plastid to cause defective development. Additionally, both *cpHsp70* and *mtHsp70* are essential for the translocation of important proteins across the inner membranes of chloroplasts and mitochondria in vivo (D'Silva et al., 2004; Su and Li, 2010). Therefore, *Bnams4*^{b} might partially impair such membrane transport systems, probably resulting in the failed transport of specific chlorophyll and fatty acid synthesis-related proteins into the tapetal plastid stroma and the chloroplast and leading to the malfunction of tapetal plastids and male sterility or to the variable frequencies of albino leaves and buds.

The ability of *Bnams4*^{b} to function in other species will likely make it a valuable research tool with multiple potential prospects for practical applications. In *A. thaliana*, *Bnams4*^{b} causes stable, complete sterility. Plants with normal leaves but sterile anthers could be isolated among such transgenic plants, suggesting that a stable male-sterile line might be derived by the inclusion of the dominant sterile gene *Bnams4*^{b} in Brassicaceae species. Notably, the sterility in *A. thaliana* could be reversed by *BnaC9.Tic40*. This indicated that restorer lines could potentially be derived using *BnaC9.Tic40* in *A. thaliana*. Therefore, it might be possible to introduce ideal agronomic traits into male sterile or restorer lines to rapidly cultivate superior hybrids. We are in the process of determining whether this system might potentially be available in other species such as the dicotyledons tobacco (*Nicotiana tabacum*) and cotton (*Gossypium hirsutum*) and in the monocotyledon rice (*Oryza sativa*). Overall, the fertility conversion system described herein, which consists of two co-evolved genes, shows considerable potential value for future transgenic breeding.

METHODS

Plant Materials and Growth Conditions

The NIL 7365AC (*Bnams3ms3ms4*^{b}*ms4*^{c}/*Bnams3ms3ms4*^{c}*ms4*^{c}) was obtained by repeated backcrossing for map-based cloning of *Bnams4*^{b}, construction of a BAC library, genetic transformation, RT-PCR, transcriptome sequencing, small RNA sequencing, cuticle analysis, and cytological observations. Two hundred varieties of *Brassica napus* were provided by Yongming Zhou in Huazhong Agricultural University. A total of 148 inbred lines of *B. napus* were conserved in our laboratory. These two populations of *B. napus*, collected in 2009 and 2014, respectively, were representative inbred lines or natural pure-lines used for association mapping with various genetic backgrounds. Wild-type Col-0 *Arabidopsis thaliana* was used for genetic transformation, GUS analysis, and subcellular localization analysis. Diverse basic species were collected from the Centre for Genetic Resources, Plant Genetic Resources, The Netherlands (CGN-PGR) (Supplemental Data Set 1). Information on other experimental materials can be found in the following method. Transgenic *B. napus* and *A. thaliana* plants were grown in the greenhouse under conditions of 20 to 22°C and 16/8 h night/day). Nontransgenic *B. napus* plants were grown under normal farming practices in the field of Huazhong Agricultural University, Hubei, China.

Physical Fine Mapping of *Bnams4*^{b}

The sterile gene *Bnams4*^{b} was defined in a physical region 304 kb in size according to the published genome sequence of *B. rapa* (Wang et al., 2011b; Xia et al., 2012). The candidate region of *Bnams4*^{b} (namely, *BnRf*) had favorable genomic synteny with Scaffold000017 of the *B. rapa* genome, but limited synteny with the *A. thaliana* genome (Xia et al., 2012). Therefore, a series of sequence characterized amplified regions and simple sequence repeat markers were designed according to the nucleotide sequence of Scaffold000017 to narrow down the physical region of *Bnams4*^{b} (Xia et al., 2012). Mixed pools of DNA from sterile and fertile plants were used to screen polymorphic markers linked to *Bnams4*^{b} as described (Dun et al., 2011). The genetic distances of the polymorphic markers were determined using 5500 NIL 7365AC individuals. The nearest flanking markers, CL14 and DD42, located *Bnams4*^{b} to 85-kb (Figure 2B) and 78-kb (Figure 2C) DNA fragments according to the *Chiifu-401* and *Darmor-bzh* genome sequences, respectively. This smaller physical region contained four candidate genes. Although these four genes have not been previously characterized or predicted to be involved in anther development, the respective complete sequences of the four genes in the *Bnams4*^{b} candidate region were cloned. These represented four candidate genes for *Bnams4*^{b}. Each of the four candidate genes for *Bnams4*^{b} was transformed into fertile 7365C (*Bnams3ms3ms4*^{c}*ms4*^{c}) plants and wild-type Col-0 *A. thaliana*. None of the transgenic plants had a sterile phenotype.

We were unable to amplify the intergenic sequence between two of the four candidate genes. Therefore, thermal asymmetric interlaced-PCR was repeatedly performed to clone the intergenic sequence in the *Bnams4*^{b} candidate region as described (Li et al., 2013). Finally, ~15 kb was obtained, from which markers were developed and screened. Using a population of 5500 individuals, we further identified several cosegregated markers to screen the BAC clone library of 7365AC (SD2F-SD1R). All PCR products were separated on 6% polyacrylamide denaturing gels. Bands were visualized with a silver-staining method (Yi et al., 2006) or separated on 0.8 to 1% agarose gels and visualized with an agarose gel imaging system (Bio-Rad). The primer sequences used for mapping *Bnams4*^{b} are listed in Supplemental Table 1.

Construction of a BAC Library and the Screening, Sequencing, and Assembling of the Target Monoclone

The BAC clone library was constructed according to a previously described method (Luo and Wing, 2003). We cooperated with COSETE Technology Company to complete the construction of the BAC library. After the seeds were sown, seedlings with very small leaves were grown under weak light for ~10 d. To prepare high molecular weight genomic DNA fragments (average length of ~700 kb), ~150 g of fresh pale green leaves was ground in liquid N_2 in a mortar until small tissue chunks could be seen. This process was followed by gentle mixing of the incubated nuclear suspensions at 45°C for 5 min with 1% low-melting-temperature agarose prepared in NIB and preincubated at 45°C. The mixture was added to plug molds and placed on ice for ~40 min to form plugs. After the preparation of genomic DNA plugs, each half DNA plug (50 μL) was chopped into fine pieces and transferred to a microcentrifuge tube containing 45 μL of restriction enzyme buffer and was incubated on ice for 40 min. Gradient dilutions of restriction enzyme were used. The microcentrifuge tubes were then incubated in a 37°C water bath for 40 min. CHEF agarose gels were used to separate the digested product. DNA fragments of 90 to 110 kb were selected to perform DNA ligation. CopyControl pCC1BAC (HindIII Cloning-

Ready) Vector (cat. no. CBAC311H) was used for ligation with selected DNA fragments. The ligation product was transformed into thawed ElectroMax DH10B T1 phage-resistant competent cells in prechilled electroporation cuvettes. Gradient volume transformation solutions of each culture were plated on 150-mm-diameter Petri dish agar plates. The number of recombinant clones was adjusted to 800 to 1000 per Petri dish. We calculated the average length of the insertion to be ~93 kb (Supplemental Figure 15). The colonies were collected into a 2-mL centrifuge tube to obtain mixed BAC clones pools. Ultimately, we obtained 100 mixed pools, and the genome size contained in this BAC library was 93 kb × 900 clones × 100 pools (~7.982 Gb).

Plasmids from each mixed pool were extracted using the protocol described by Sambrook and Russell (2001). The primer pairs 4F3DF-4F3DR and SD2F-SD1R were used to screen the target monoclone containing the *Bnams4*^{b} locus. Serial numbers of clone pools identified by 4F3DF-4F3DR were 5, 6, 7, 17, 33, 37, 49, and 58. Those identified by SD2F-SD1R were 5, 35, 46, 58, 80, and 100. We sequenced the amplified fragments and confirmed number 58 to be a candidate BAC pool, which we used to screen the final monoclone containing *Bnams4*^{b}. Gradient dilutions of 5-, 10-, and 50-fold after a 10,000-fold dilution of mixed bacteria pools of the number 58 were plated on 150-mm-diameter Petri dish agar plates; then the monoclones (nearly 800 to 1000 per dish) were picked using a toothpick-dipping method to identify those containing *Bnams4*^{b} (Schenk, 2014). B107 was the final monoclone that contained *Bnams4*^{b}. Plasmid extraction from B107 was performed with a Qiagen Large-Construct Kit (cat. no. 12462). The protocol used to construct the sequencing library for the BAC plasmid was provided by the high-throughput sequencing facility (HiSeq 2000 platform) at the State Key Laboratory of Crop Genetic Improvement. Paired-end sequencing was performed with ~1 Gb per monoclone. SOAP (BGI Technology) was used for sequence assembly.

Plasmid Construction and Complementation Transformation

Vector construction for the complementation test and *B. napus* transformation was performed as described (Dun et al., 2011). All fragments for vector construction were amplified by Phusion DNA Polymerase (F-530S; Thermo Scientific). The four candidate genes showing sequence similarity with *Bra014988*, *Bra014989*, *Bra014990*, and *Bra014991* were cloned into the vector pCAMBIA2300 using the traditional digestion and ligation method with restriction endonuclease and T4 ligase, respectively. Each construct contained a native promoter (~2 kb), exons, introns, and 3′ sequence (~1 kb). The whole sequence of CC4 (containing a 1906-bp promoter, nine exons, eight introns, and an 1185-bp 3′ sequence) was cloned into the vector pCAMBIA2300. For *Bnams4*^{a}, the same method was adopted as used for CC4. To further confirm the function of the *Bnams4*^{b} ORF, two other vectors were constructed with the *A9* (At5g07230) promoter (1199 bp) and *RBCS* (At1g67090) promoter (1061 bp), followed by the *Bnams4*^{b} ORF using pMDC83 binary vector. The primers used for promoter-GUS analysis were GUSF and GUSR (Supplemental Table 1). GUSR was designed close to the translation initiation site with no base gap. The length of GUSFR amplification was 2084 bp. This fragment was cloned into the PBI101 promoter-GUS analysis vector using a suitable restriction enzyme. To reconstruct the pollination control system in *A. thaliana*, the whole sequence of *BnaC9.Tic40* (containing a 1951-bp promoter, 14 exons, 13 introns, and a 1227-bp 3′ sequence) was cloned into the vector pCAMBIA2300 to recover sterility by *Bnams4*^{b} (CC4). Detailed procedures of *B. napus Agrobacterium tumefaciens*-mediated transformation using the hypocotyls infection method followed those previously described (Yi et al., 2010). Agrobacterium-mediated transformation of *A. thaliana* was performed using the floral-dip method (Clough and Bent, 1998).

Subcellular Localization of *Bnams4*^{b}

To determine the subcellular localization of the Bnams4^{b} protein, an *A. thaliana* protoplast transformation assay and Agrobacterium-mediated transient expression of tobacco leaf epidermal cells were employed. These two subcellular localization assays were performed according to published methods, with some modifications (Sparkes et al., 2006; Yoo et al., 2007). For the *A. thaliana* protoplast transformation assay, two segmental *Bnams4*^{b} ORFs (AA1 and AA1+AA2, 657 and 1557 bp, respectively; Figure 4A) starting from the translation initiation site were inserted individually into a GFP-fusion expression vector pM999-35S-GFP. PEG-calcium-mediated transfection was used to deliver DNA into the *A. thaliana* protoplast, followed by a 5- to 24-h incubation to for gene expression (Yoo et al., 2007). RFP fusion with the chaperone binding protein BIP was used as an additional endoplasmic reticulum marker protein (Kim et al., 2001). Chloroplast autofluorescence was artificially changed to a blue color. For Agrobacterium-mediated transient expression by *Nicotiana tabacum*, the two segments were individually cloned into another GFP-fusion expression vector, pMDC83. The mGFP6 sequence in this pMDC83 vector was replaced with a pM999-GFP sequence using *Kpn*I and *Sac*I. Expression of these two fusion genes in greenhouse-grown 6-week-old tobacco leaves was achieved by agroinfiltration (~0.6 OD) with GV3101 harboring pMDC83-AA1 and pMDC83-(AA1+AA2). Fluorescence of GFP and RFP were visualized using a FluoView FV1000 laser scanning confocal microscope (Olympus). Conditions for imaging were set at 488-nm excitation, collecting bandwidth at 500 to 520 nm for GFP and 559-nm excitation, collecting bandwidth at 570 to 583 nm for RFP.

5′, 3′ RACE and Confirmation of *Bnams4*^{b} Gene Structure

RACE was performed using the GeneRacer Kit (for full-length, RNA ligase-mediated rapid amplification of 5′ and 3′ cDNA ends; catalog no. L1502-01). Total RNA from sterile buds of *Bnams4*^{b} transgenic *A. thaliana* and buds of sterile plants in 7365AC was reverse transcribed into cDNA. After amplifying the cDNA ends of each sample, nested PCR was performed to obtain the terminal sequences. The full-length cDNAs of *Bnams4*^{b} were submitted to NCBI BLAST-N to confirm the exact sequences of eight introns according to conservative exon sequences of related species in the NCBI database (http://blast.ncbi.nlm.nih.gov/Blast.cgi?CMD=WebandPAGE_TYPE=BlastHome). The rules of eukaryotic intron initiation and termination sequences were used to examine the authenticity of start and stop bases of *Bnams4*^{b} introns. Meanwhile, deep transcriptome sequencing data of the 7365A anther (the stage of abortion with 11 to 2-mm buds) was also used to check the authenticity of eight intron sequences (Figure 7D).

RT-qPCR and Immunoblotting

Total RNAs from albino leaves of varying degrees from transgenic *B. napus*, various tissues from NIL 7365AC sterile plants, and anthers of three genotypes from self-crossing of fertile individuals in NIL 736512AB were isolated using TRIzol reagent (Invitrogen) according to the user manual. One or two micrograms of RNA from each sample was reverse transcribed to cDNA using the SuperScript III reverse transcriptase (Invitrogen) or RevertAid First Strand cDNA Synthesis Kit (#K1622; Thermo Fisher Scientific). To guarantee the specification of quantitative primers, we first designed consensus primers to amplify the transcribed cDNA of buds, then sequenced the bands and compared them to the sequence of *Bnams4*^{b} cDNA. Next, specific quantitative primers of *Bnams4*^{b} were designed to perform RT-PCR and RT-qPCR. RT-PCR procedures were performed as described (Zhou et al., 2012). qRT-PCR was performed on an CFX96TM real-time system (C1000 thermal cycler; Bio-Rad) using SYBR Green Realtime PCR Master Mix (QPK-201; TOYOBO) and Hard-Shell PCR plates (catalog: HSP9655; Bio-Rad). For each sample, the experiment was performed with four technical replicates or three biological replicates. *Bnaactin3* and *A. thaliana ACTIN2* were used as the reference genes for normalization in *B. napus* and Arabidopsis samples, respectively. For RT-PCR of microsamples, buds (0.3 to 0.6 mm, tetrad stage) and siliques

(4 d after pollination) from wild-type and transgenic *A. thaliana* were collected for total RNA extraction using the SV Total RNA Isolation and Purification System (Z3100; Promega). RNA isolation from transgenic and 7365AC anthers (1- to 2-mm buds) were performed with the same kits. Reverse transcription of these RNAs was performed by RevertAid First Strand cDNA Synthesis Kit (#K1622; Thermo Fisher Scientific). RT-PCR primers are listed in Supplemental Table 1.

For immunoblotting, the *Bnams4*^{b} fragment was amplified from the cDNA of sterile buds using the primers WB-F and WB-R. The pGEX-4T-3 vector (GE Healthcare Life Sciences) was used to construct pGEX-4T-3-*Bnams4*^{b}. The purified fusion protein was used as the antigen. The antibody was prepared by ABclonal Technology. Immunoblot experiments were performed as previously described (Jing et al., 2012). Total protein (0.1 g) of five albino cauline leaves from independent transgenic *B. napus* lines was extracted using extraction buffer (0.1 mmol/L Tris-HCl, 0.1 mmol/L EDTA, 0.15 mol/L NaCl, and 0.5% butanol, pH 7.5 to 8.0). β-Actin (for plants, AC009) was used as an endogenous standard.

Bisulfite Sequencing and McrBC PCR

DNA extraction (anthers from the tetrad period of *Bnams3ms3ms4*^{a}*ms4*^{a} and *Bnams3ms3ms4*^{b}*ms4*^{b} genotypes, ~1.5 mm) was performed following the Qiagen DNeasy Plant Mini Kit (cat. no. 69106) handbook. A sample of 500 ng genomic DNA was treated for sodium bisulfite conversion using the Qiagen EpiTect Bisulfite kit (cat. no. 59104). Control primers NADFR were used to check the samples were treated adequately (Supplemental Table 1). DNA purification was performed using the Qiagen PCR purification kit (cat. no. 28106). Primers for bisulfate sequencing PCR were designed using Kismeth (https://phytozome.jgi.doe.gov/pz/portal.html#!search?show=BLAST; Supplemental Table 1). Amplification, cloning, and sequencing were performed as previously described (Wang et al., 2011a). DNA cytosine methylation in the CG, CHG, and CHH sites were analyzed on the above website.

McrBC-PCR experiments were performed as previously described (Ding et al., 2007; Rabinowicz et al., 2003). Digestion was performed by McrBC enzyme following the instruction (M0272S; New England Biolabs). PCR amplifications were performed using equal amounts of McrBC-digested and nondigested DNA of the anthers from the three genotypes of plants. Real-time McrBC-PCR was performed to quantitatively measure the methylation level. The primers for these experiments can be found in Supplemental Table 1.

Analysis of Anther Wax and Cutin

Wax and cutin from four types of anther epidermis, derived from three genotypes and two developmental stages, were analyzed as previously described (Jung et al., 2006; Li et al., 2010). Six different univariate linear regression equations were generated to estimate the ratios of dried anther weight-to-surface area (Supplemental Figure 16). Area was determined from pixel numbers in microscopy images, assuming the *B. napus* anthers to possess a cylindrical body. To extract wax, 6 to 10 mg of each sample of freeze-dried anther material was submersed in 1 mL chloroform for 1 min. Ten milligrams of tetracosane (Fluka) was used as an internal standard and was added to the resulting chloroform extracts and transferred to new vials. After evaporation under a gentle stream of nitrogen gas, free hydroxyl and carboxyl groups were converted to their trimethylsilyl ethers and esters by adding 20 mL of BSTFA (*N*,*N*-bis-trimet hylsilyltrifluoroacite amide; Macherey-Nagel) and 20 mL of pyridine to the extracts, which were then incubated for 40 min at 70°C. The remaining delipidated anthers were dried over silica gels and used to analyze the monomer composition of cutin polyester as described (Franke et al., 2005). The final data were subjected to one-way ANOVA F test for each comparison (Supplemental Figure 17).

Measurement of Chlorophyll

An SPAD-502 meter (Konica-Minolta) and a spectrophotometer (Mapada; UV-1800) were used to measure the chlorophyll concentration in *Bnams4*^{b} transgenic and wild-type *A. thaliana* leaves. Two wild-type individuals and two albino individuals were measured during flowering. The SPAD values were converted to absolute units of chlorophyll concentration (total chlorophyll per unit fresh weight; mg/g, R^2 = 0.9809) according to calibration equations ($y = 0.0007x^2 + 0.0230x + 0.0544$) (Ling et al., 2011). Photometric measurements of solvent-extracted chlorophyll were performed according to a method previously described (Lichtenthaler, 1987). Five technical replicates of each experiment were performed.

Characterization of Anther Phenotypes

TEM analysis was performed as described (Li et al., 2006). Anthers from buds of various sizes from sterile and fertile plants in 7365AB and cut leaves (2 mm) were prefixed and vacuumized in 2.5% (w/v) glutaraldehyde with 0.1 M phosphate buffer (pH 7.4). After the anthers sank, the samples were kept in the refrigerator at 4°C. Samples were fixed in 2% OsO_4, dehydrated, embedded, and used to generate ultrathin sections as previously described (Li et al., 2006). Scanning electron microscopy and the generation of semithin sections were performed as previously described (Yi et al., 2010; Zhu et al., 2010). The stages of anther development in this study were distinguished according to the methods described in a previous study (Sanders et al., 1999).

Phylogenetic Analysis and Sequence Divergence Estimation

The amino acid sequence of *Bnams4*^{b} was divided into three sections (AA1, AA2, and AA3) and then used for BLAST searches against the phytozome (https://phytozome.jgi.doe.gov/pz/portal.html#!search?show=BLAST) with relative species. Homologous sequences in *B. napus* (http://www.genoscope.cns.fr/brassicanapus/), *B. rapa* (*Brams4*^{b}), and *B. oleracea* (http://www.ocri-genomics.org/bolbase/) were added manually. Multiple homologous sequences were derived and aligned with Clustal Omega (http://www.ebi.ac.uk/Tools/msa/clustalo/). Three maximum likelihood phylogenetic trees were obtained by aligning homologous protein sequences of the three sections with those in related species using the MEGA package version 6.0.6 (Tamura et al., 2013), and the LG+G model with all gaps deleted. Bootstrap values were obtained from 1000 replicates. The same method was used to perform phylogenetic analysis of whole sequences of *Bnams4*^{b} homologs in the four species after removing the corresponding nucleotide sequences of the 490 amino acids in *Bol029014*. The divergence times of Tic40s among *Brassica* species, *A. thaliana*, *Arabidopsis lyrata*, and *Capsella rubella* were estimated by MEGA 6.0. Nucleotide substitution rate was set as 1.5×10^{-8} (Koch et al., 2000). Four times were used as molecular clock calibration: calibration name = '*B. rapa* and *B. oleracea*', MinTime = 3.60000000 and MaxTime = 5.60000000 (Liu et al., 2014); calibration name = '*A. thaliana* and *A. lyrata*', MinTime = 3.00000000 and MaxTime = 5.80000000 (Koch and Matschinger, 2007); calibration name = '*C. rubella* and *A thaliana*', MinTime = 5.00000000 and MaxTime = 9.00000000 (Franzke et al., 2009; German et al., 2009); calibration name = '*A thaliana* and *B. rapa*', MinTime = 14.00000000 and MaxTime = 24.00000000 (Yang et al., 1999). All sequence data used to analyze phylogeny relationships or divergence times were provided with a FASTA format in a sequence compressed file (Supplemental Files 1 to 5).

Anther mRNA Transcriptome Sequencing and Small RNA Sequencing

Total RNA samples of three kinds of anthers from self-crossing progeny of fertile individuals in NIL 736512AB were used for mRNA transcriptome and small RNA sequencing. Anthers from the tetrad period (buds 1.5 to 2 mm) were used for analysis. mRNA sequencing was performed on the HiSeq 2000 platform at the State Key Laboratory of Crop Genetic Improvement.

Three libraries corresponding to three samples were sequenced producing 30-Gb clean data (~10 Gb per library). Small RNA sequencing was performed by Novogene in Beijing; three libraries corresponding to three samples were sequenced producing 5.60 Gb clean data (1.94, 1.70, and 1.87 Gb). The reference sequence in IGV was the B107 BAC sequence. Parameters of the reads matched those of the reference sequence by 100%. Small RNA reads with <19 or >24 nucleotides were excluded for IGV mapping.

Yeast Two-Hybrid Assays

Gal4-based yeast two-hybrid assay was performed using the Matchmaker Gold Yeast Two-Hybrid System from Clontech according to the manufacturer's instructions. Full-lengths CDS of BnaC9.Tic40, BnaC9.tic40, and Bnams4^{b} were cloned into the PGBKT7 vector (GAL4-BD domain) and the PGADT7 vector (GAL4-AD domain) (primers are listed in Supplemental Table 1), respectively. The pairs of constructs were cotransformed into AH109 yeast cells and dropped on synthetic dropout nutrient medium (SD/-Trp-Leu-His-Ade) or (SD/-Trp-Leu, as positive control) agar plates.

Accession Numbers

Sequence data from this article can be found in the Arabidopsis Genome Initiative or GenBank/EMBL databases under the following accession numbers: *Bnams4^{a}*, KX756983; *Bnams4^{b}*, KX756984; *Bol029014*, KX756985; *Bnaactin3*, LOC106418315; and *ACTIN2*, AT3G18780.

Supplemental Data

Supplemental Figure 1. The sterility and albino phenotypes of transformed wild-type *A. thaliana* and 7365C by *CC4*.

Supplemental Figure 2. Relative expression levels of *Bnams4^{b}* in both transgenic *A. thaliana* and transgenic *B. napus* tissues.

Supplemental Figure 3. The nucleotide sequence of *Bnams4^{b}*.

Supplemental Figure 4. Sterile phenotypes of *Bnams4^{b}*-transgenic *A. thaliana* driven by the *A. thaliana A9* promoter.

Supplemental Figure 5. Chloroplast localization of Bnams4^{b} protein by Agrobacterium-mediated transient expression in tobacco leaf epidermal cells.

Supplemental Figure 6. Semithin sections of fertile and sterile anthers in NIL 7365AC.

Supplemental Figure 7. TEM examination of fertile and sterile anthers in NIL 7365AC.

Supplemental Figure 8. Maximum likelihood phylogenetic trees summarizing the evolutionary relationships among the Bnams4^{b}-related proteins (AA1, AA2, and AA3).

Supplemental Figure 9. Amino acid alignment of Brams4^{b}-40, Bnams4^{b}, and Bol029014.

Supplemental Figure 10. The estimated divergence times of Tic40s among *Brassica* species, *A. thaliana*, *A. lyrata*, and *C. rubella* by MEGA 6.0.

Supplemental Figure 11. Wild-type *A. thaliana* flower and transgenic flowers carrying the *Bnams4^{a}ms4^{a}* allele that differs by two SNPs.

Supplemental Figure 12. Small RNA regions of all three genotypes showed high-level DNA methylation by McrBC-PCR.

Supplemental Figure 13. Comparison of sequence collinearity between partial BAC sequence of *Bnams4^{b}* and sequence corresponding to *Bnams4^{c}ms4^{c}* by Unipro UGENE.

Supplemental Figure 14. Bnams4^{b} could not directly interact with BnaC9.Tic40 and BnaC9.tic40.

Supplemental Figure 15. Average insert size assay of the BAC library of 7365AC.

Supplemental Figure 16. Linear regression equations of anther dry weight and anther surface area with sterile and fertile anthers of different genotypes and developmental stages.

Supplemental Figure 17. Simple ANOVA tables in this study.

Supplemental Table 1. Primers used in this study.

Supplemental Table 2. Homology and annotations of genes in candidate region.

Supplemental Table 3. Amino acid and nucleotide identities between *Bnams4^{b}* and its intact homologous genes in *B. rapa*, *B. oleracea*, *B. napus*, and *B. juncea*

Supplemental Table 4. Number of individuals containing *Bnams4^{b}* or *BnaMs3* in F1 and F2 transgenic *A. thaliana*.

Supplemental Table 5. Neutral selection tests of *Bnams4^{b}* by Mcdonald-Kreitman[1], Tajima's D[2], and Fu and Li[3].

Supplemental Table 6. Detection of positive selection of seven *ms4^{b}* homologous genes in *B. napus*, *B. rapa*, *B. oleracea*, and *B. juncea*.

Supplemental File 1. Fifteen homologous sequences of AA1 in Brassicaceae.

Supplemental File 2. Thirty-one homologous sequences of AA2 in Brassicaceae.

Supplemental File 3. Thirty-eight homologous sequences of AA3 in Brassicaceae.

Supplemental File 4. Thirteen homologous sequences of *Bnams4^{b}* in Brassicaceae.

Supplemental File 5. tic40 homologous sequences in Brassicaceae.

Supplemental Data Set 1. The information for diverse Brassicaceae accessions.

Supplemental Data Set 2. Ka/Ks value and divergence time of Tic homologous genes estimated by DnaSP.

ACKNOWLEDGMENTS

We thank Hanhui Kuang and Yidan OuYang (Huazhong Agricultural University) for helpful discussions. This research was supported by funds from the National Key R&D Program for Crop Breeding (2016YFD0100305), the National Natural Science Foundation of China (31130040), National Natural Science Funds of China (31501374), China postdoctoral Science Foundation (2015M570646), and the Natural Science Foundation of Hubei province Key program (2014CFA008).

AUTHOR CONTRIBUTIONS

S.X. wrote the initial draft of the manuscript and performed all of the experiments involving the map-based cloning, cytological observation, expression, and biochemical analysis. Z.W. participated in the genetic transformation work. H.Z. participated in the genotype frequencies investigation and statistical analysis and contributed to partial genetic transformation. K.H. analyzed the sequence data and performed the phylogenetic and dN/dS ratio analyses. M.Q. performed the immunoblotting. Z.Z. participated in subcellular localization. X.D. supplied the sequence information on *BnaC9.Tic40* orthologs. B.Y., J.W., C.M., J.S., and T.F. supervised the study. J.T. conceived and supervised the writing.

Received April 11, 2016; revised July 19, 2016; accepted August 24, 2016; published August 24, 2016.

REFERENCES

Bédard, J., Kubis, S., Bimanadham, S., and Jarvis, P. (2007). Functional similarity between the chloroplast translocon component, Tic40, and the human co-chaperone, Hsp70-interacting protein (Hip). J. Biol. Chem. **282:** 21404–21414.

Betrán, E., Thornton, K., and Long, M. (2002). Retroposed new genes out of the X in Drosophila. Genome Res. **12:** 1854–1859.

Bonaventure, G., Beisson, F., Ohlrogge, J., and Pollard, M. (2004). Analysis of the aliphatic monomer composition of polyesters associated with Arabidopsis epidermis: occurrence of octadeca-cis-6, cis-9-diene-1,18-dioate as the major component. Plant J. **40:** 920–930.

Capra, J.A., Pollard, K.S., and Singh, M. (2010). Novel genes exhibit distinct patterns of function acquisition and network integration. Genome Biol. **11:** R127.

Cardoso-Moreira, M., and Long, M. (2012). The origin and evolution of new genes. Methods Mol. Biol. **856:** 161–186.

Chalhoub, B., et al. (2014). Plant genetics. Early allopolyploid evolution in the post-Neolithic *Brassica napus* oilseed genome. Science **345:** 950–953.

Chen, F.X., Hu, B.C., and Li, Q.S. (1993). Discovery and Study of Genic Male Sterility(GMS) Material 9012 A in *Brassica napus* L. Acta Agric. Univ. Pekinensis **19:** 57–61.

Chen, F.X., Hu, B.C., Li, Q.S., Hou, S.M., Wu, X.J., and Fei, W.X. (2002). The breeding of the recessive epistatically genic male sterile hybrid rapeseed-Wanyou18 with double low. Journal of Anhui Agricultural Sciences **30:** 535–537.

Chen, F.X., Hu, B.C., Li, Q.S., Hou, S.M., Wu, X.J., Fei, W.X., Li, C., and Chen, W.S. (2003). Breeding of Wanyou 14, a recessive epistatically genic male sterile hybrid rapeseed (Brassica napus) with double low. Chinese Journal of Oil Crop Sciences **25:** 63–65.

Chen, S., Zhang, Y.E., and Long, M. (2010). New genes in Drosophila quickly become essential. Science **330:** 1682–1685.

Chen, S., Krinsky, B.H., and Long, M. (2013). New genes as drivers of phenotypic evolution. Nat. Rev. Genet. **14:** 645–660.

Chen, S., Spletter, M., Ni, X., White, K.P., Luo, L., and Long, M. (2012a). Frequent recent origination of brain genes shaped the evolution of foraging behavior in Drosophila. Cell Reports **1:** 118–132.

Chen, S., Ni, X., Krinsky, B.H., Zhang, Y.E., Vibranovski, M.D., White, K.P., and Long, M. (2012b). Reshaping of global gene expression networks and sex-biased gene expression by integration of a young gene. EMBO J. **31:** 2798–2809.

Chen, W., Yu, X.H., Zhang, K., Shi, J., De Oliveira, S., Schreiber, L., Shanklin, J., and Zhang, D. (2011). Male Sterile2 encodes a plastid-localized fatty acyl carrier protein reductase required for pollen exine development in Arabidopsis. Plant Physiol. **157:** 842–853.

Chou, M.L., Chu, C.C., Chen, L.J., Akita, M., and Li, H.M. (2006). Stimulation of transit-peptide release and ATP hydrolysis by a cochaperone during protein import into chloroplasts. J. Cell Biol. **175:** 893–900.

Chou, M.L., Fitzpatrick, L.M., Tu, S.L., Budziszewski, G., Potter-Lewis, S., Akita, M., Levin, J.Z., Keegstra, K., and Li, H.M. (2003). Tic40, a membrane-anchored co-chaperone homolog in the chloroplast protein translocon. EMBO J. **22:** 2970–2980.

Clough, S.J., and Bent, A.F. (1998). Floral dip: a simplified method for Agrobacterium-mediated transformation of Arabidopsis thaliana. Plant J. **16:** 735–743.

de Azevedo Souza, C., Kim, S.S., Koch, S., Kienow, L., Schneider, K., McKim, S.M., Haughn, G.W., Kombrink, E., and Douglas, C.J. (2009). A novel fatty Acyl-CoA synthetase is required for pollen development and sporopollenin biosynthesis in Arabidopsis. Plant Cell **21:** 507–525.

Dennis, M.Y., et al. (2012). Evolution of human-specific neural SRGAP2 genes by incomplete segmental duplication. Cell **149:** 912–922.

Ding, Y., Zhou, Q., and Wang, W. (2012). Origins of new genes and evolution of their novel functions. Annu. Rev. Ecol. Evol. Syst. **43:** 345–363.

Ding, Y., Wang, X., Su, L., Zhai, J., Cao, S., Zhang, D., Liu, C., Bi, Y., Qian, Q., Cheng, Z., Chu, C., and Cao, X. (2007). SDG714, a histone H3K9 methyltransferase, is involved in Tos17 DNA methylation and transposition in rice. Plant Cell **19:** 9–22.

Ding, Y., Zhao, L., Yang, S., Jiang, Y., Chen, Y., Zhao, R., Zhang, Y., Zhang, G., Dong, Y., Yu, H., Zhou, Q., and Wang, W. (2010). A young Drosophila duplicate gene plays essential roles in spermatogenesis by regulating several Y-linked male fertility genes. PLoS Genet. **6:** e1001255.

D'Silva, P., Liu, Q., Walter, W., and Craig, E.A. (2004). Regulated interactions of mtHsp70 with Tim44 at the translocon in the mitochondrial inner membrane. Nat. Struct. Mol. Biol. **11:** 1084–1091.

Dun, X., Zhou, Z., Xia, S., Wen, J., Yi, B., Shen, J., Ma, C., Tu, J., and Fu, T. (2011). BnaC.Tic40, a plastid inner membrane translocon originating from Brassica oleracea, is essential for tapetal function and microspore development in *Brassica napus*. Plant J. **68:** 532–545.

Dun, X., Shen, W., Hu, K., Zhou, Z., Xia, S., Wen, J., Yi, B., Shen, J., Ma, C., Tu, J., Fu, T., and Lagercrantz, U. (2014). Neofunctionalization of duplicated Tic40 genes caused a gain-of-function variation related to male fertility in *Brassica oleracea* lineages. Plant Physiol. **166:** 1403–1419.

Fan, Q.X., Meng, D.Q., Tang, T.Z., Li, Z.F., Xu, L., and Liu, N. (2010). Effect of fertilizer and density on the yield of Mianyou 63. Anhui Agric. Sci. Bull. **16:** 93–94.

Franke, R., Briesen, I., Wojciechowski, T., Faust, A., Yephremov, A., Nawrath, C., and Schreiber, L. (2005). Apoplastic polyesters in Arabidopsis surface tissues–a typical suberin and a particular cutin. Phytochemistry **66:** 2643–2658.

Franzke, A., German, D., Al-Shehbaz, I.A., and Mummenhoff, K. (2009). Arabidopsis family ties: molecular phylogeny and age estimates in Brassicaceae. Taxon **58:** 425–437.

German, D.A., Friesen, N., Neuffer, B., Al-Shehbaz, I.A., and Hurka, H. (2009). Contribution to ITS phylogeny of the Brassicaceae, with special reference to some Asian taxa. Plant Syst. Evol. **283:** 33–56.

Goldman, N., and Yang, Z. (1994). A codon-based model of nucleotide substitution for protein-coding DNA sequences. Mol. Biol. Evol. **11:** 725–736.

Grainger, R.J., and Beggs, J.D. (2005). Prp8 protein: at the heart of the spliceosome. RNA **11:** 533–557.

Heinen, T.J.A.J., Staubach, F., Häming, D., and Tautz, D. (2009). Emergence of a new gene from an intergenic region. Curr. Biol. **19:** 1527–1531.

Huang, Z., Xiao, L., Dun, X.L., Xia, S.Q., Yi, B., Wen, J., Shen, J.X., Ma, C.Z., Tu, J.X., Meng, J.L., and Fu, T.D. (2012). Improvement of the recessive genic male sterile lines with a subgenomic background in Brassica napus by molecular marker-assisted selection. Mol. Breed. **29:** 181–187.

Jarosz, D.F., and Lindquist, S. (2010). Hsp90 and environmental stress transform the adaptive value of natural genetic variation. Science **330:** 1820–1824.

Jing, B., Heng, S., Tong, D., Wan, Z., Fu, T., Tu, J., Ma, C., Yi, B., Wen, J., and Shen, J. (2012). A male sterility-associated cytotoxic protein ORF288 in Brassica juncea causes aborted pollen development. J. Exp. Bot. **63:** 1285–1295.

Jones, C.D., and Begun, D.J. (2005). Parallel evolution of chimeric fusion genes. Proc. Natl. Acad. Sci. USA **102:** 11373–11378.

Jung, K.H., Han, M.J., Lee, D.Y., Lee, Y.S., Schreiber, L., Franke, R., Faust, A., Yephremov, A., Saedler, H., Kim, Y.W., Hwang, I., and An, G. (2006). Wax-deficient anther1 is involved in cuticle and wax production in rice anther walls and is required for pollen development. Plant Cell **18:** 3015–3032.

Kim, D.H., Eu, Y.J., Yoo, C.M., Kim, Y.W., Pih, K.T., Jin, J.B., Kim, S.J., Stenmark, H., and Hwang, I. (2001). Trafficking of phosphatidylinositol 3-phosphate from the trans-Golgi network to the lumen of the central vacuole in plant cells. Plant Cell **13:** 287–301.

Koch, M.A., and Kiefer, M. (2005). Genome evolution among cruciferous plants: a lecture from the comparison of the genetic maps of three diploid species–*Capsella rubella*, *Arabidopsis lyrata* subsp. petraea, and *A. thaliana*. Am. J. Bot. **92:** 761–767.

Koch, M.A., and Matschinger, M. (2007). Evolution and genetic differentiation among relatives of *Arabidopsis thaliana*. Proc. Natl. Acad. Sci. USA **104:** 6272–6277.

Koch, M.A., Haubold, B., and Mitchell-Olds, T. (2000). Comparative evolutionary analysis of chalcone synthase and alcohol dehydrogenase loci in Arabidopsis, Arabis, and related genera (Brassicaceae). Mol. Biol. Evol. **17:** 1483–1498.

Lamesch, P., et al. (2012). The Arabidopsis Information Resource (TAIR): improved gene annotation and new tools. Nucleic Acids Res. **40:** D1202–D1210.

Li, F., Yan, L., Lai, J., Ma, C., Gautam, M., and Fu, T. (2013). Molecular cloning and mRNA expression profile of sucrose transporter gene BnSUT1C from *Brassica napus* L. Indian J. Exp. Biol. **51:** 1130–1136.

Li, H., Pinot, F., Sauveplane, V., Werck-Reichhart, D., Diehl, P., Schreiber, L., Franke, R., Zhang, P., Chen, L., Gao, Y., Liang, W., and Zhang, D. (2010). Cytochrome P450 family member CYP704B2 catalyzes the omega-hydroxylation of fatty acids and is required for anther cutin biosynthesis and pollen exine formation in rice. Plant Cell **22:** 173–190.

Li, N., et al. (2006). The rice tapetum degeneration retardation gene is required for tapetum degradation and anther development. Plant Cell **18:** 2999–3014.

Lichtenthaler, H.K. (1987). Chlorophylls and carotenoids:pigments of photosynthetic biomembranes. Methods Enzymol. **148:** 350–382.

Ling, Q., Huang, W., and Jarvis, P. (2011). Use of a SPAD-502 meter to measure leaf chlorophyll concentration in *Arabidopsis thaliana*. Photosynth. Res. **107:** 209–214.

Liu, S., et al. (2014). The *Brassica oleracea* genome reveals the asymmetrical evolution of polyploid genomes. Nat. Commun. **5:** 3930–3941.

Long, M., and Langley, C.H. (1993). Natural selection and the origin of jingwei, a chimeric processed functional gene in Drosophila. Science **260:** 91–95.

Luo, M., and Wing, R.A. (2003). An improved method for plant BAC library construction. Methods Mol. Biol. **236:** 3–20.

Lysak, M.A., Koch, M.A., Pecinka, A., and Schubert, I. (2005). Chromosome triplication found across the tribe Brassiceae. Genome Res. **15:** 516–525.

Lysak, M.A., Berr, A., Pecinka, A., Schmidt, R., McBreen, K., and Schubert, I. (2006). Mechanisms of chromosome number reduction in *Arabidopsis thaliana* and related Brassicaceae species. Proc. Natl. Acad. Sci. USA **103:** 5224–5229.

Marhold, K., and Lihova, J. (2006). Polyploidy, hybridization and reticulate evolution: lessons from the Brassicaceae. Plant Syst. Evol. **259:** 143–174.

Matsuno, M., et al. (2009). Evolution of a novel phenolic pathway for pollen development. Science **325:** 1688–1692.

Nagaharu, U. (1935). Genomic anlaysis in Brassica with special reference to the experimental formation of B. napus and peculiar mode of fertilization. Jpn. J. Bot. **7:** 389–452.

Parker, H.G., et al. (2009). An expressed fgf4 retrogene is associated with breed-defining chondrodysplasia in domestic dogs. Science **325:** 995–998.

Queitsch, C., Sangster, T.A., and Lindquist, S. (2002). Hsp90 as a capacitor of phenotypic variation. Nature **417:** 618–624.

Rabinowicz, P.D., Palmer, L.E., May, B.P., Hemann, M.T., Lowe, S.W., McCombie, W.R., and Martienssen, R.A. (2003). Genes and transposons are differentially methylated in plants, but not in mammals. Genome Res. **13:** 2658–2664.

Rogers, R.L., Bedford, T., and Hartl, D.L. (2009). Formation and longevity of chimeric and duplicate genes in Drosophila melanogaster. Genetics **181:** 313–322.

Rohner, N., Jarosz, D.F., Kowalko, J.E., Yoshizawa, M., Jeffery, W.R., Borowsky, R.L., Lindquist, S., and Tabin, C.J. (2013). Cryptic variation in morphological evolution: HSP90 as a capacitor for loss of eyes in cavefish. Science **342:** 1372–1375.

Rutherford, S.L., and Lindquist, S. (1998). Hsp90 as a capacitor for morphological evolution. Nature **396:** 336–342.

Sambrook, J., and Russell, D.W. (2001). Molecular Cloning: A Laboratory Manual, 3rd ed. (Cold Spring Harbor, NY: Cold Spring Harbor Laboratory Press).

Sanders, P.M., Bui, A.Q., Weterings, K., McIntire, K., Hsu, Y.-C., Lee, P.Y., Truong, M.T., Beals, T., and Goldberg, R. (1999). Anther developmental defects in *Arabidopsis thaliana* male-sterile mutants. Sex. Plant Reprod. **11:** 297–322.

Sayah, D.M., Sokolskaja, E., Berthoux, L., and Luban, J. (2004). Cyclophilin A retrotransposition into TRIM5 explains owl monkey resistance to HIV-1. Nature **430:** 569–573.

Schenk, P.M. (2014). Rapid cloning of genes and promoters for functional analyses. Methods Mol. Biol. **1099:** 123–132.

Schranz, M.E., Lysak, M.A., and Mitchell-Olds, T. (2006). The ABC's of comparative genomics in the Brassicaceae: building blocks of crucifer genomes. Trends Plant Sci. **11:** 535–542.

Schwartz, B.W., Yeung, E.C., and Meinke, D.W. (1994). Disruption of morphogenesis and transformation of the suspensor in abnormal suspensor mutants of Arabidopsis. Development **120:** 3235–3245.

Shi, J., et al. (2011). Defective pollen wall is required for anther and microspore development in rice and encodes a fatty acyl carrier protein reductase. Plant Cell **23:** 2225–2246.

Sollars, V., Lu, X., Xiao, L., Wang, X., Garfinkel, M.D., and Ruden, D.M. (2003). Evidence for an epigenetic mechanism by which Hsp90 acts as a capacitor for morphological evolution. Nat. Genet. **33:** 70–74.

Sparkes, I.A., Runions, J., Kearns, A., and Hawes, C. (2006). Rapid, transient expression of fluorescent fusion proteins in tobacco plants and generation of stably transformed plants. Nat. Protoc. **1:** 2019–2025.

Su, P.H., and Li, H.M. (2010). Stromal Hsp70 is important for protein translocation into pea and Arabidopsis chloroplasts. Plant Cell **22:** 1516–1531.

Sun, C.C., Zhao, H., Wang, W.R., Li, Y.L., Qian, X.F., and Fang, G.H. (2004). Breeding of a recessive genic male sterile (GMS) hybrid variety HuyouzaNo.1 with double low in *Brassica napus* L. Zhongguo You Liao Zuo Wu Xue Bao **26:** 63–65.

Tamura, K., Stecher, G., Peterson, D., Filipski, A., and Kumar, S. (2013). MEGA6: Molecular Evolutionary Genetics Analysis version 6.0. Mol. Biol. Evol. **30:** 2725–2729.

Wang, J., Wang, C., Long, Y., Hopkins, C., Kurup, S., Liu, K., King, G.J., and Meng, J. (2011a). Universal endogenous gene controls for bisulphite conversion in analysis of plant DNA methylation. Plant Methods **7:** 39–45.

Wang, W., Brunet, F.G., Nevo, E., and Long, M. (2002). Origin of sphinx, a young chimeric RNA gene in *Drosophila melanogaster*. Proc. Natl. Acad. Sci. USA **99:** 4448–4453.

Wang, W., et al. (2006). High rate of chimeric gene origination by retroposition in plant genomes. Plant Cell **18:** 1791–1802.

Wang, W.R., Sun, C.C., Li, Y.L., Zhou, X.R., Zhuang, J., Yang, L.Y., Jiang, M.Y., and Jin, Q.L. (2009). Breeding of the Brassica napus cultivar Huyouza 4, a recessive genic male sterile (GMS) hybrid with double low content in rapeseed. Shanghai Nong Ye Xue Bao **25:** 69–71.

Wang, X., et al.; Brassica rapa Genome Sequencing Project Consortium (2011b) The genome of the mesopolyploid crop species *Brassica rapa*. Nat. Genet. **43:** 1035–1039.

Weng, J.K., Li, Y., Mo, H., and Chapple, C. (2012). Assembly of an evolutionarily new pathway for α-pyrone biosynthesis in Arabidopsis. Science **337:** 960–964.

Xia, S., Cheng, L., Zu, F., Dun, X., Zhou, Z., Yi, B., Wen, J., Ma, C., Shen, J., Tu, J., and Fu, T. (2012). Mapping of BnMs4 and BnRf to a common microsyntenic region of *Arabidopsis thaliana* chromosome 3 using intron polymorphism markers. Theor. Appl. Genet. **124:** 1193–1200.

Yang, Y.W., Lai, K.N., Tai, P.Y., and Li, W.H. (1999). Rates of nucleotide substitution in angiosperm mitochondrial DNA sequences and dates of divergence between Brassica and other angiosperm lineages. J. Mol. Evol. **48:** 597–604.

Yi, B., Chen, Y., Lei, S., Tu, J., and Fu, T. (2006). Fine mapping of the recessive genic male-sterile gene (Bnms1) in *Brassica napus* L. Theor. Appl. Genet. **113:** 643–650.

Yi, B., Zeng, F., Lei, S., Chen, Y., Yao, X., Zhu, Y., Wen, J., Shen, J., Ma, C., Tu, J., and Fu, T. (2010). Two duplicate CYP704B1-homologous genes BnMs1 and BnMs2 are required for pollen exine formation and tapetal development in *Brassica napus*. Plant J. **63:** 925–938.

Yogeeswaran, K., Frary, A., York, T.L., Amenta, A., Lesser, A.H., Nasrallah, J.B., Tanksley, S.D., and Nasrallah, M.E. (2005). Comparative genome analyses of Arabidopsis spp.: inferring chromosomal rearrangement events in the evolutionary history of *A. thaliana*. Genome Res. **15:** 505–515.

Yoo, S.D., Cho, Y.H., and Sheen, J. (2007). Arabidopsis mesophyll protoplasts: a versatile cell system for transient gene expression analysis. Nat. Protoc. **2:** 1565–1572.

Zhan, Z.B., Zhang, Y., Zhao, R.P., and Wang, W. (2011). [Evolutionary fate and expression patterns of chimeric new genes in *Drosophila melanogaster*]. Zool. Res. **32:** 585–595.

Zhang, C., Wang, J., Xie, W., Zhou, G., Long, M., and Zhang, Q. (2011). Dynamic programming procedure for searching optimal models to estimate substitution rates based on the maximum-likelihood method. Proc. Natl. Acad. Sci. USA **108:** 7860–7865.

Zhou, Z., Dun, X., Xia, S., Shi, D., Qin, M., Yi, B., Wen, J., Shen, J., Ma, C., Tu, J., and Fu, T. (2012). BnMs3 is required for tapetal differentiation and degradation, microspore separation, and pollen-wall biosynthesis in *Brassica napus*. J. Exp. Bot. **63:** 2041–2058.

Zhu, Y., Dun, X., Zhou, Z., Xia, S., Yi, B., Wen, J., Shen, J., Ma, C., Tu, J., and Fu, T. (2010). A separation defect of tapetum cells and microspore mother cells results in male sterility in *Brassica napus*: the role of abscisic acid in early anther development. Plant Mol. Biol. **72:** 111–123.